Journal of Materials Chemistry B

ROYAL SOCIETY OF CHEMISTRY

PERSPECTIVE

View Article Online
View Journal | View Issue

Check for updates

Cite this: J. Mater. Chem. B, 2024, 12, 2720

Trends in bioactivity: inducing and detecting mineralization of regenerative polymeric scaffolds

Brandon M. Nitschke,[a] Felipe O. Beltran,[b] Mariah S. Hahn[c] and Melissa A. Grunlan *[abd]

Received 10th November 2023,
Accepted 14th February 2024

DOI: 10.1039/d3tb02674d

rsc.li/materials-b

Due to limitations of biological and alloplastic grafts, regenerative engineering has emerged as a promising alternative to treat bone defects. Bioactive polymeric scaffolds are an integral part of such an approach. Bioactivity importantly induces hydroxyapatite mineralization that promotes osteoinductivity and osseointegration with surrounding bone tissue. Strategies to confer bioactivity to polymeric scaffolds utilize bioceramic fillers, coatings and surface treatments, and additives. These approaches can also favorably impact mechanical and degradation properties. A variety of fabrication methods are utilized to prepare scaffolds with requisite morphological features. The bioactivity of scaffolds may be evaluated with a broad set of techniques, including *in vitro* (acellular and cellular) and *in vivo* methods. Herein, we highlight contemporary and emerging approaches to prepare and assess scaffold bioactivity, as well as existing challenges.

1. Introduction

1.1. Current methods to treat bone defects

Bone tissue is critical for mechanical functionality, protection, and hematopoiesis.[1,2] These traits stem from its unique combination of carbonated hydroxyapatite (HAp) [$Ca_{10}(PO_4)_6(OH)_2$] embedded in an extracellular matrix (ECM) comprised of collagen (primarily type I), proteoglycans, and glycoproteins. While capable of regeneration, bone tissue healing is limited for defects beyond a critical size that stem from traumatic injury, surgical excision, or congenital anomalies.[3] Bone tissue healing is also hindered by advanced age, osteoarthritis, and radiological treatment. Numerous products have been developed to treat and heal critical-sized bone defects, and are exemplified in Table 1.

Biological grafting approaches are frequently employed, wherein the living tissue graft becomes incorporated into the surrounding tissue. Autografting remains the 'gold standard' with over two million bone autografts performed annually.[4] However, autografting is associated with complex surgical harvesting (*e.g.*, from tibia or iliac crest), donor site morbidity, and limited availability, as well as premature resorption stemming from poor contact with adjacent tissue. Cadaveric allografts are also associated with limited availability and premature resorption, as well as immune rejection.[4] Xenografts, particular bovine grafts, have been explored but pose a risk for disease transmission, a greater chance of host immune response, highly variable resorption rates, and reduction in osteoinductive properties due to strict manufacturing and processing requirements.[5,6] Alloplastic bone substitutes have been leveraged as an alternative to biological grafts. For example, demineralized bone matrix (DBM) is prepared *via* decalcification (*i.e.*, removal of HAp) of cortical bone allografts with an acidic solution that leaves behind a composite of collagens, non-collagenous proteins, growth factors, residual calcium phosphate mineral (1–6%), and trace cellular debris.[7] Alloplastic grafts have also been prepared based on one or more synthetic bioactive "bioceramics", including: bioactive glasses (BGs),[8,9] HAp[10–12] β-tricalcium phosphate [β-$Ca_3(PO_4)_2$; β-TCP],[13,14] and calcium sulfate.[15] Silicate BGs are widely used for their capacity to bond to bone, and represent certain compositions of SiO_2–Na_2O–CaO–P_2O_5 (*e.g.*, 45S5-BG). In the granular form, DBM and bioceramics provide advantageous microporosity and complete resorption. Still, these are also often combined with a polymer coating or matrix to afford injectability or moldability within irregular shapes, as well as to circumvent brittleness in certain cases.[16] The use of poly(methyl methacrylate) (PMMA) is associated with exothermic cures, post-cure shrinkage, lack of porosity, and non-degradability, as well as brittle mechanical properties.[17,18] To mitigate brittleness and afford replacement by neotissue, numerous degradable synthetic and natural polymers have been employed.[19–22] Synthetic polyesters and copolymers

[a] Department of Biomedical Engineering, Texas A&M University, College Station, TX 77843, USA. E-mail: mgrunlan@tamu.edu
[b] Department of Materials Science & Engineering, Texas A&M University, College Station, TX 77843, USA
[c] Department of Biomedical Engineering, Rensselaer Polytechnic Institute, Troy, NY 12180, USA
[d] Department of Chemistry, Texas A&M University, College Station, TX 77843, USA

Table 1 Examples of commercial biological and alloplastic materials to treat bone defects

Product name	Bioactive component	Matrix/carrier component
AlloFuse® (AlloSource)	DBM	Reverse phase medium gel
Calcigen® S (Zimmer Biomet)	Calcium sulfate	Not reported
Cerament® (BONESUPPORT)	HAp & calcium sulfate	Not reported
CranioSculpt™ (KLS Martin)	Calcium phosphate	Not reported
Cortoss® (Stryker)	Bioactive glass ceramic	Acrylate copolymer
Grafton™ DBM (Medtronic)	DBM	Glycerol
Kinex® (Globus Medical)	BG	Collagen, hyaluronic acid
MinerOss® (BioHorizons)	Cortical & cancellous bone chips	None
NanoFUSE® (Amend Surgical)	DBM & BG-45S5 coated with gelatin	None
Optium® (LifeNet Health)	DBM	Glycerol
OSferion (Arthrex)	β-TCP	None
Osteosponge® (XTANT Medical)	DBM	None
Puros® (ZimVie)	DBM	Reverse phase medium gel
Vestakeep® Fusion (Evonik)	Biphasic calcium phosphate	PEEK

thereof have been widely utilized given the tunability of properties.[20] More recently, polyether ether ketone (PEEK) 3D printed alloplastic devices have been created in complex, patient-specific geometries,[23] including as composites with bioactive fillers.[24,25]

1.2. Regenerative engineering approaches with bioactive scaffolds

Owing to the limitations of biological and alloplastic grafts, regenerative engineering approaches have emerged to heal bone defects.[26] The scaffold compositions play an instrumental role, and must fulfill a demanding set of criteria to maximize bone tissue healing.[27,28] Bioactivity is of significant importance as it leads to the formation of HAp that promotes osteogenic differentiation (*i.e.*, osteoinductivity), as well as osseointegration with surrounding bone tissue (Fig. 1).[29–31]

While bioactive HAp is innately present in biological grafts, for alloplastic grafts, bioactivity is traditionally afforded by the inclusion of DBM or bioceramics. Scaffolds that are potently bioactive may reduce or even eliminate the necessity of exogeneous growth factors (*e.g.*, bone morphogenic protein 2, BMP-2), which risk off-target responses.[32] Beyond bioactivity, the scaffold must also be osteoconductive (*i.e.*, permitting cell migration and neotissue infiltration).[33,34] This is achieved through porosity that may be afforded through a variety of fabrication methods (*e.g.*, 3D printing, solvent cast particulate leaching [SCPL], gas foaming, freeze drying, and electrospinning) with polymers forming the regenerative bone scaffold.[35] Degradation of the scaffold also facilitates osteoconductivity, making the rate of scaffold resorption important to healing. To enable osseointegration, the scaffold must form close contact with adjacent bone tissue.[29] This has been particularly addressed with injectable scaffolds,[36] 3D-printed scaffolds,[37,38] and shape memory polymer (SMP) scaffolds.[39]

2. Imparting bioactivity to scaffolds

Given the importance of bioactivity to bone regeneration, bioactive polymeric scaffolds continue to be developed (Fig. 2). Approaches include bioactive composite scaffolds based on combining polymers with bioactive fillers (*e.g.*, DBM and bioceramics), bioactive coatings and surface treatments, as well as surface modification of scaffolds. Recent reports are exemplified herein.

2.1. Bioactive composite scaffolds

Bioactive composite scaffolds, comprised of one or more bioceramics embedded in a polymer matrix,[40–42] remain prolific in regenerative bone engineering. *Versus* bioceramic-only scaffolds, these composites can improve processibility, increase rigidity and strength, and mitigate brittleness that contribute to post-surgical fracture. Furthermore, owing to the hydrophilicity and susceptibility to hydrolysis, bioceramic–polymer composites also degrade at favorably faster rates compared to polymer-only scaffolds. A variety of bioactive composite scaffolds have recently been reported (Table 2). Both biodegradable

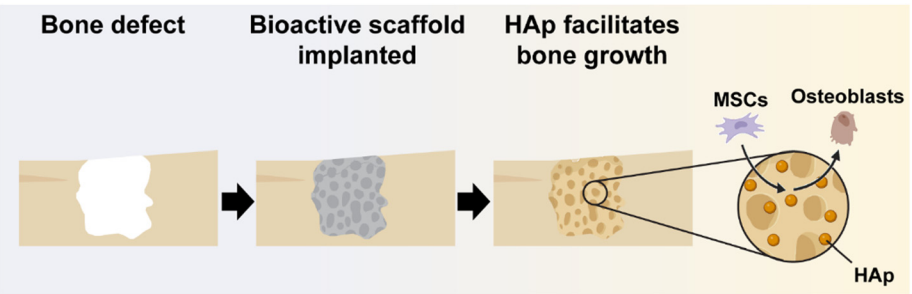

Fig. 1 Bioactive scaffolds lead to HAp mineralization, and subsequently promote osteogenesis and osseointegration.

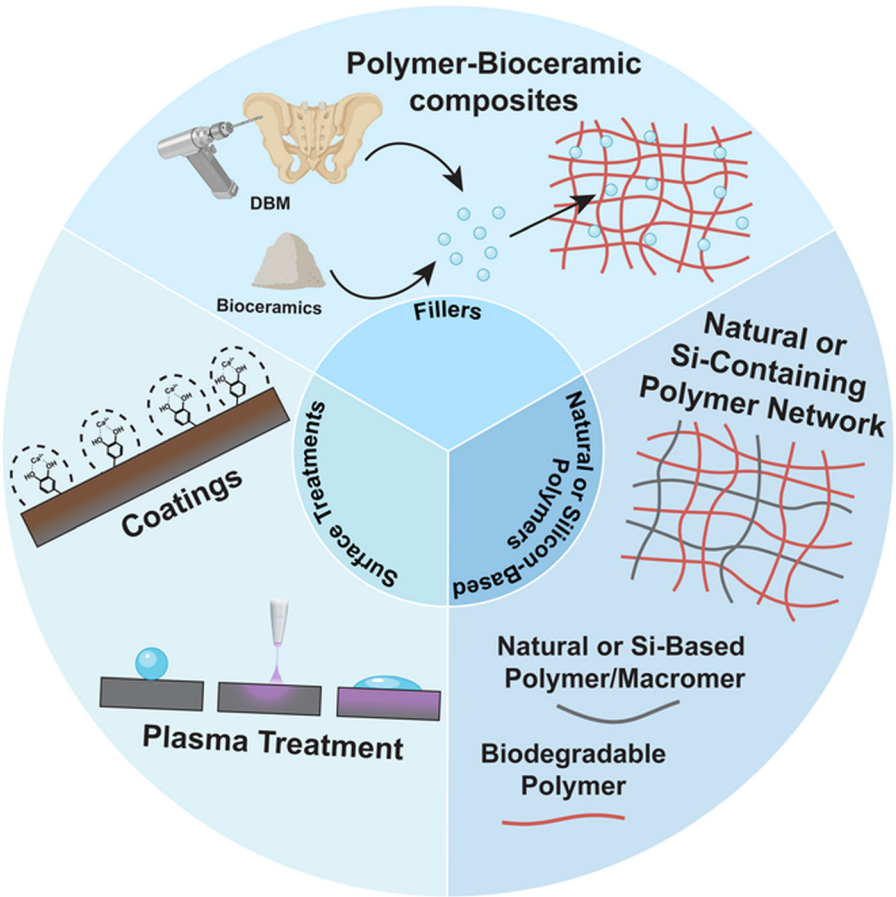

Fig. 2 Methods to prepare bioactive polymeric scaffolds for bone regeneration.

synthetic and natural polymers have been utilized. A variety of bioceramics and glasses have been leveraged, ranging from historically used types (*e.g.*, BG, HAp, and β-TCP), to newer types (*e.g.*, nanosilicates, and eggshell particles). Their mineralization activity and mechanism vary, with some capable of acellular mineralization in physiological environments including simulated body fluid (SBF) (Fig. 3). For instance, 45S5-BG [45 wt% SiO_2, 24.5 wt% Na_2O, 24.5 wt% CaO, and 6 wt% P_2O_5] is known to promote rapid HAp formation on its surface within hours.[43] The mechanism involves a series of sequential steps: (1) exchange of Na^+ ions with solution H^+, (2) hydrolysis of Si–O–Si bonds to form SiOH bonds, and the release of $Si(OH)_4$, (3) polycondensation to form a hydrated silica gel, (4) formation of an amorphous calcium phosphate phase *via* absorption of Ca^{2+}, PO_4^{3-}, and CO_3^{2-} ions, and (5) crystallization to carbonated HAp. Synthetic HAp is also capable of inducing the formation of a HAp layer in SBF, and at greater levels *versus* BG-45S5.[44] HAp forms through several steps: (1) adsorption of Ca^{2+} ions to the surface, (2) formation of Ca-rich amorphous calcium phosphate at surface, (3) transition to a Ca-poor surface due to adsorption of solution PO_4^{3-} as well as CO_3^{2-} ions, and (4) crystallization into carbonated HAp.[45] In addition to bone bonding, the formed HAp layer facilitates bone formation *via* the stimulation of mesenchymal stem cell (MSC) osteogenesis, especially *via* increased expression of growth factors (*e.g.*, BMP) and enhanced alkaline phosphatase (ALP) activity. In contrast, β-TCP does not mineralize with SBF exposure, but rather is osteoconductive and osteoinductive.[14] β-TCP leads to osteoclast-mediated resorption and osteoconduction that is associated with rapid bone formation and high bone bonding strengths.

For bioactive composite scaffolds, the level of incorporated bioactive bioceramics is highly variable, ranging from less than 1 wt% to over 50 wt%. Composites prepared with two or more distinct types of bioceramics have also been reported. A number of fabrication methods have been employed (*e.g.*, SCPL, electrospinning). Notably, various forms of 3D printing have been leveraged extensively to impart finer control of microarchitecture as well as to produce patient-specific scaffolds.[46] For instance, selective laser sintering (SLS) 3D printing employs a laser to sinter a powder (*e.g.*, a mixture of polymer and bioceramic) and fuse particles together, while unfused particles support the structure. Comparison of composite scaffold bioactivity efficacy is difficult, as *in vitro* and *in vivo* evaluations of such scaffolds are highly variable in the literature. For example, time-points selected to confirm HAp mineralization following exposure to SBF vary appreciably (from 1 day to several weeks). Still, some studies directly compare scaffolds prepared with two different bioceramics.

Table 2 Examples of bioactive composite scaffolds for bone regeneration

Study	Bioactive component	Matrix component	Wt% of Filler	Fabrication method	Key findings
Shuai, 2021[47]	HAp	PLLA, or PGA	10%	3D printing (SLS)	HAp/PLLA/PGA scaffolds displayed tunable degradation and mechanical properties.
Xu, 2017[48]	HAp or β-TCP	PLGA	50%	SCPL	HAp/PLGA scaffolds exhibited higher strength and faster degradation; TCP/PLGA scaffolds improved bone regeneration in a rabbit model.
Cheng, 2021[49]	β-TCP (with cucurbitacin B)	PLGA	25%	3D printing (low temperature rapid prototyping)	TCP/PLGA/Cur-B scaffolds increased bone regeneration and angiogenesis in a rat model.
Nyberg, 2017[50]	HAp, β-TCP, DBM, or BO	PCL	30%	3D printing (extrusion)	DBM/PCL and BO/PCL scaffolds exhibited greater osteoinduction; PCL/HAp displayed higher compressive modulus.
Shuai, 2022[51]	PDLA-grafted HAp (*g*-HAp)	PDLA	0.5, 1, 2 or 4%	3D printing (SLS)	*g*-HAp/PDLA scaffolds exhibited increased modulus and strength.
Sultan, 2022[52]	45S5-BG	PLA	5%	TIPS and 3D printing (extrusion)	45S5-BG/PLA scaffolds exhibited increased strength.
Nitschke, 2023[53]	45S5-BG	PCL, PLLA	2.5 to 30%	Modified SCPL	45S5-BG/SMP scaffolds exhibited faster degradation, and retained shape memory behavior.
Distler, 2020[54]	45S5-BG	PLA	1–10 wt%	FDM	45S5-BG/PLA scaffolds exhibited decreased strength with increased BG wt%; triggered cellular osteogenesis.
Monfared, 2022[55]	45S5-BG and β-TCP	Gelatin, and PVA	35–40% (equal parts each)	3D printing (extrusion)	45S5-BG/TCP/Gelatin/PVA scaffolds exhibited increased compressive strength and faster degradation.
Han, 2023[56]	BBG	PCL	5–40%	3D printing (SLS)	BBG/PCL scaffolds with 20 wt% BGG exhibited optimal mechanical properties, and promoting regeneration & integration in a rabbit model.
Hatton, 2019[57]	ICIE16M-BG	Alginate	50%	Freeze-drying	ICI16M-BG/alginate scaffolds exhibited increased strength.
Du, 2019[58]	MBG	SF, or PCL	80%	3D printing (extrusion)	MBG/SF exhibited superior compressive strength, and greater heterotopic bone formation in a mouse model.
Qi, 2017[59]	MBG and calcium sulfate	PCL	70%	3D printing (extrusion)	MBG/CS scaffolds exhibited superior osteogenesis of cultured human bone marrow mesenchymal stem cells (hBMSCs) and greater bone formation in a rat model.
Carrow, 2019[60]	LAPONITE®	PEOT/PBT	5, 10, or 15%	3D printing (extrusion)	LAPONITE®/PEOT/PBT scaffolds exhibited decreased degradation rates *versus* copolymer-only scaffolds, as well as increased osteogenesis of hMSCs.
Wu, 2021[61]	Eggshell microparticles (ESP)	Gel–MA	ESP combined with 5% prepolymer solution	Casting/UV cure	ESP/Gel–MA scaffolds exhibited superior osteogenesis of cultured MC3T3-E1 pre-osteoblasts *versus* Gel–MA-only scaffold, and greater bone formation in a rat model.
Huang, 2020[62]	MWCNTs &/or nHAp	PCL	0.75% MWCNT & 20% nHAp	3D printing (screw assisted extrusion)	PCL/MWCNT/nHAp scaffolds exhibited increased modulus *versus* PCL-only scaffolds, and greater osteogensis of cultured hADSCs.

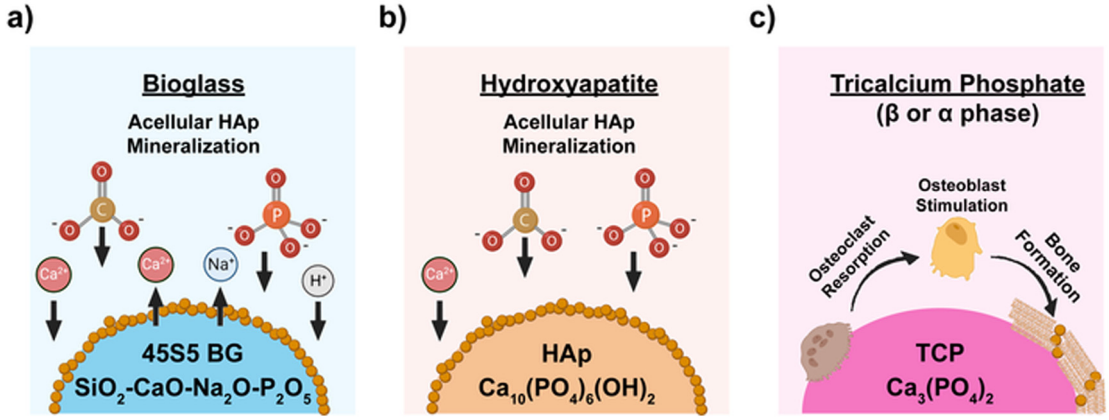

Fig. 3 Simplified mechanisms of mineralization for common bioceramics: (a) BG-45S5, (b) synthetic HAp, and (c) β-TCP.

Both HAp and β-TCP continue to be utilized to prepare bioactive composite scaffolds, either alone or in combinations. Shuai *et al.* utilized SLS 3D printing to fabricate composite scaffolds based on HAp (10 wt%) with poly(L-lactic acid) (PLLA) and poly(glycolic acid) (PGA).[47] *Versus* HAp/PLLA composite scaffolds, the faster degradation of HAp/PLLA/PGA composites (50 : 50 wt% PLLA : PGA) enhanced the exposure of HAp, leading to superior mineralization and regeneration in a rabbit segmental defect model. Xu *et al.* reported both HAp- and β-TCP-containing poly(lactic-*co*-glycolic acid) (PLGA) composite scaffolds *via* SCPL.[48] Compressive tests revealed that HAp-scaffolds had higher strengths and rates of *in vitro* degradation compared to β-TCP-scaffolds. In a rabbit calvarial defect, while early-stage bone growth was faster for HAp-scaffolds, β-TCP-scaffolds exhibited greater bone mineral densities and higher compressive strengths of repaired bone at 20 weeks. Cheng *et al.* introduced cucurbitacin B, a plant-derived terpene, to β-TCP/PLGA scaffolds leading to enhanced osteogenesis and neovascularization.[49] In an example by Nyberg *et al.*, a series of 3D printed composite poly(ε-caprolactone) (PCL) scaffolds were prepared by altering the bioactive filler: a bioceramic (HAp or β-TCP) or a biologic (decellularized bone matrix [DBM] or Bio-Oss® [BO], a clinically available form of DBM).[50] BO/PCL and DBM/PCL scaffolds exhibited enhanced osteoinduction *versus* HAp/PCL and TCP/PCL scaffolds, while the compressive modulus was highest for HAp/PCL scaffolds. Shuai *et al.* reported poly(D,L-lactic acid) (PDLLA) grafted onto HAp (*g*-HAp), combined with PLLA to prepare composite scaffolds *via* SLS 3D printing.[51] As a result of improved interfacial bonding *via* stereo-complexation, *g*-HAp/PLLA composite scaffolds displayed significant enhancements in stiffness and strength.

BGs continue to be utilized to prepare bioactive composite scaffolds. Sultan *et al.* prepared composite scaffolds based on 45S5-BG (5 wt%) and poly(lactic) acid (PLA).[52] Thermally induced phase separation (TIPS) was used to create a homogenous distribution of BG, and the resulting composite spheres were subsequently formed into scaffolds *via* extrusion 3D printing. Due to the homogeneous distribution of BG, scaffold compressive strength increased for printed scaffolds.

We have previously reported 'self-fitting' SMP scaffolds based on PCL,[63] including PCL/PLLA semi-interpenetrating networks (semi-IPNs).[64] Recently, Nitschke *et al.* reported analogous composite scaffolds that included 45S5-BG.[53] A modified SCPL protocol was utilized wherein the fused template was formed from a mixture of BG and salt, resulting in localization of BG on the scaffold pore walls. At just 5 and 10 wt% BG, 45S5-BG/PCL scaffolds induced HAp mineralization after 1 day in SBF (1X), and degraded faster *versus* corresponding polymer-only scaffolds, all while maintaining shape memory behavior. Distler *et al.* described 45S5-BG/PLA scaffolds with 1–10 wt% BG formed by fused deposition modeling (FDM) of 45S5-BG/PLA filaments.[54] Monfared *et al.* combined 45S5-BG with β-TCP (50 : 50 wt% ratio; 35–45 wt% total) to prepare composite scaffolds based on gelatin, poly(vinyl alcohol) (PVA), and Tween® 60 using extrusion-based 3D printing.[55] The printed scaffolds achieved higher moduli *versus* analogous scaffolds prepared by foam casting.

Newer types of bioceramics have also been developed and used to prepare bioactive composite scaffolds. For example, borate-containing BGs (BBGs), wherein borate (B_2O_3) is partially or completely substituted for silica (SiO_2), are associated with faster rates of HAp formation compared to silicate bioactive glasses (*e.g.*, 45S5).[65] Thus, BBG composite scaffolds have been formed, as in Han *et al.* wherein BBG/PCL scaffolds were prepared by SLS 3D printing.[56] Furthermore, ICIE16-BG, a potassium-containing BG (48.0 SiO_2, 6.6 Na_2O, 32.9 CaO, 2.5 P_2O_5, 10.0 K_2O [wt%]), was developed as an alternative to 45S5-BG.[57] For instance, Hatton *et al.* combined ICIE16-BG with alginate to form composite scaffolds *via* freeze-drying.[66] Still, different types of bioactive silicate bioceramics have been leveraged to form bioactive composite scaffolds. Mesoporous bioactive glasses (MBG) based on silicates have well-defined pores with diameters around 5 to 20 nm, presenting a large surface area.[67] Du *et al.* 3D printed composite scaffolds from MBG (80 wt%) combined with silk fibroin (SF) and PCL, with MBG/SF scaffolds exhibiting superior strength and bioactivity *versus* MBG/PCL scaffolds.[58] While relatively low cost, calcium sulfate exhibits particularly rapid resorption as well as limited

bioactivity.[68] Thus, Qi *et al.* prepared 3D printed scaffolds wherein MBG and calcium sulfate were combined with PCL.[59] In addition to MBG, other nanosized bioactive fillers have also been utilized to form bioactive scaffolds,[69] including HAp nanoparticles,[70] and nanosilicates (*e.g.*, LAPONITE®).[71,72] Carrow *et al.* reported 3D printed scaffolds using LAPONITE® in combination with a poly(ethylene oxide terephthalate) (PEOT)/poly(butylene terephthalate) (PBT) (PEOT/PBT) copolymer.[60] Wu *et al.* reported the use of chicken eggshell microparticles (ESP), possessing high levels of calcium and representing a sustainable alternative to BGs, to form bioactive composite scaffolds in combination with gelatin methacrylate (Gel–MA).[61] To achieve biomimetic scaffolds in terms of not only bioactivity but structure, Huang *et al.* prepared PCL scaffolds with multi-walled carbon nanotubes (MWCNTs) and nano-HAp (nHAp), using screw-assisted extrusion based 3D printing to align the MWCNTs.[62] Piezoelectric perovskites such as barium titanate (BTO) have also shown to be capable of HAp mineralization.[73] In the case of BTO, when exposed to an electric field or mechanical stress, the titanium and oxygen ions switch locations, leading to a concentration of negatively charged O^{2-} on the material surface. In turn, positively charged Ca^{2+} ions from the physiologic fluid are attracted to the surface, leading to the formation of an apatite layer.[74]

2.2. Bioactive coatings and surface treatments

Various bioactive coatings have historically been applied to metal implants.[75] To achieve bioactivity of polymeric scaffolds, coatings have been likewise applied.[76,77] Such coatings can enhance the bioactivity of composite scaffolds, or be used in lieu of fillers to avoid brittleness. Bioceramic coatings may also be directly applied to scaffolds. Recently, several bioactive coatings and surface treatments have been applied to scaffolds to promote bioactivity (Table 3). For instance, Fazeli *et al.* reported the deposition of HAp and BG onto 3D printed PCL scaffolds *via* an immersion method with a HAp/BG solution.[78] Zhang *et al.* reported PCL scaffolds coated with HAp *via* pulsed laser deposition (PLD).[79] Li *et al.* described HAp deposition onto PVA/PLA scaffolds *via* electrodeposition.[80] Coatings based on a combination of bioceramics and polymers have also been reported. For instance, based on the bioactivity of chitosan,[81] Shaltooki *et al.* applied a chitosan/BG coating to PCL/BG composite scaffolds by exposing scaffolds to homogenized solutions.[82] Alternatively, a bioactive polymeric coating may be applied to scaffolds. Collagen type I, a natural component of bone tissue, is a frequently used material for bone regeneration.[83] Thus, Tabatabaei *et al.* reported PCL/β-TCP scaffolds coated by collagen using an immersion method that included homogenization.[84] While developed for the purpose of assessment of biomaterial bioactivity, SBF exposure has been used to deposit bioactive mineral coatings onto polymeric scaffolds.[76,85] Polydopamine (PDA) was established to readily form adherent coatings onto substrates *via* base-catalyzed autooxidation of dopamine.[86,87] PDA was confirmed to induce HAp mineralization in SBF,[88] leading to its use as a coating to create bioactive scaffolds for bone regeneration. Numerous studies have been noted in a recent review by Tolabi *et al.*, with the scaffold polymer component frequently being a biodegradable polyester.[89] We likewise applied a PDA coating to polyester SMP scaffolds, which resulted in enhanced osteogenic differentiation of hMSCs as well as HAp mineralization after SBF exposure.[90]

Direct surface treatment of polymeric scaffolds has also been utilized to invoke bioactivity.[76,91] Plasma treatment, wherein an electric current passes through a gas (*e.g.*, oxygen, argon, and ammonia), is a popular method.[92] This process can be used to produce surface functionalization, etching, or film deposition, while maintaining scaffold bulk properties.[93] Oxygen plasma treatment has been extensively utilized, including for PCL-based scaffolds, to enhance surface hydrophilicity and surface energy for improved cellular adhesion.[94] Depending on plasma parameters and polymer type, oxygen plasma treatment can result in both surface functionalization and etching.[93] For instance, Kim *et al.* reported oxygen plasma treatment of PCL scaffolds resulting in enhanced hydrophilicity and surface roughening.[95] These scaffolds exhibited *in vitro* mineralization by cultured cells. To confirm that such surfaces also give rise to acellular mineralization, Murab *et al.* used oxygen plasma treated PCL/TCP scaffolds exposed to SBF to demonstrate that resulting –COOH groups act as nucleation sites for amorphous calcium phosphate to form HAp crystals.[96] A significant challenge of plasma generated polymeric surfaces is their age-instability, as surfaces hydrophobically recover to the untreated state within as little as hours.[109] However, some examples display improved stability. For instance, Yamada *et al.* reported oxygen plasma treated PLA-*co*-trimethylene carbonate (PLA-*co*-TMC) scaffolds whose surfaces were stable for over 2 weeks.[97] Plasma-enhanced chemical vapor deposition (PECVD) may be utilized to apply thin films, including inorganic–organic composite films.[110] However, recent reports on its use to enhance polymeric bioactivity appear scarce. Terriza *et al.* used deposition by PECVD of SiO_2 onto the surfaces of PLGA membranes, resulting in morphological changes to osteoblasts.[98] Another form of CVD, initiated CVD (iCVD), employs a combination of a volatile initiator as well as monomer(s) to produce thin films.[110] This process avoids fragmentation of organic precursors as with PECVD. Song *et al.* reported formation of a polyelectrolyte coating *via* iCVD onto HAp scaffolds that was then exposed to supersaturated HAp, resulting in mineralized scaffolds that promoted osteogenesis.[99]

2.3. Bioactive polymers as additives

As previously noted, a variety of synthetic and natural polymers are utilized to form bone tissue scaffolds. Most of these are considered "nearly inert", or lacking in bioactivity to promote bone regeneration.[111] Yet, several natural polymers (*e.g.*, collagen,[112] gelatin,[113] chitosan,[81] alginate,[114] and hyaluronic acid[115]) display bioactivity, and have thus been formed into regenerative bone scaffolds (Table 3). In addition to being used as coatings, these bioactive polymers may be used as an additive in combination with a nearly inert polymer to form the scaffold bulk or a discrete structure within the inert

Table 3 Recent studies in bioactive coatings, surface treatment, and polymers

	Study	Bioactive coating	Matrix component	Coating method	Key findings
Coatings	Fazeli, 2023[78]	HAp	PCL	Immersion in HAp solution.	HAp-coated scaffolds displayed increased osteogenesis in rat calvarial defect models.
	Zhang, 2022[79]	HAp	PCL	PLD	Increased osteogenic potential of HAp-coated scaffolds cultured with rat BMSCs, and superior bone regeneration in critical rat calvarial defects.
	Li, 2019[80]	HAp	PVA/PLA	Electrodeposition	Longer electrodeposition times resulted in increased surface roughness and higher crystallinity of HAp.
	Shaltooki, 2019[82]	Chitosan/BG	PCL	Immersion of scaffolds in chitosan/BG solution	Chitosan/BG-coated scaffolds displayed increased hydrophilicity, degradation, and osteogenic properties.
	Tabatabaei, 2022[84]	Collagen	PCL/β-TCP	Immersion in homogenized collagen solution	Collagen-coated scaffolds displayed enhanced hydration and osteogenic potential.
	Arabiyat, 2021[90]	PDA	PCL, PCL/PLLA	Submersion in PDA solution	PDA-coated PCL/PLLA scaffolds showed acellular mineralization in SBF, and higher osteogenesis with cultured h-MSCs.

		Bioactive surface treatment	Matrix component	
Surface treatment	Kim, 2014[95]	O_2 plasma	PCL	Increased hydrophilicity and surface roughness, acellular mineralization in SBF, and increased osteogenesis with cultured mouse pre-osteoblast cells (MC3T3-E1).
	Murab, 2020[96]	O_2 plasma	PCL/TCP	O_2 plasma treated scaffolds presented –COOH groups as nucleation sites for HAp formation.
	Yamada, 2021[97]	O_2 plasma	PLA-*co*-TMC	O_2 plasma scaffolds had increased surface roughness and hydrophilicity, and improved osteogenesis of cultured rat BMSCs.
	Terriza, 2014[98]	PECVD	PLGA	15 nm SiO_2 film deposition onto PLGA films produced changes to osteoblast morphology.
	Song, 2023[99]	iCVD	HAp	iCVD treatment coated scaffolds with a polyelectrolyte induced mineralization and enhanced osteogenesis of cultured MC3T3-E1s.

		Bioactive additive	Matrix component	Scaffold fabrication method	
Bioactive additives	Jose, 2009[100]	Collagen	PLGA	Electrospinning	Increased elastic modulus for crosslinked collagen, especially for PLGA/collagen 80/20.
	Wang, 2021[101]	Gelatin	PCL	MEW and SE	Increased hydrophilicity and osteogenic potential *in vitro* compared to PCL-only nanofibers.
	Amiryaghoubi, 2022[102]	Chitosan	PCL/PU	Freeze-drying method	PCL/PU/chitosan scaffolds exhibited increased hydrophilicity, surface roughness, and promoted osteogenic differentiation of hBMSCs.
	Ren, 2021[103]	Fibrin/alginate	PCL	MEW of PCL followed by coating with FA foam	PCL/FA scaffolds exhibited superior angiogenesis in an *in vitro* model and increased bone regeneration in rat cranial defects.
	Jang, 2020[104]	Hyaluronic acid	PCL	Spray-precipitation of microspheres	PCL/HA microspheres exhibited increased osteogenic potential *in vitro* and bone regeneration after implantation in critically sized calvarial defect in a rat model.
	Frassica, 2019[105]	$PDMS_{star}$–MA	PEG–DA	Solvent induced phase separation (SIPS)	$PDMS_{star}$/PEG hydrogels displayed acellular mineralization in SBF, and osteogenesis of hBMSCs.
	Frassica, 2020[106]	PPMS–DA	PEG–DA	SIPS	PPMS/PCL scaffolds exhibited superior osteogenic potential *in vitro* compared to PEG and PEG/PDMS scaffolds.
	Beltran, 2021[107]	PDMS–DMA	PCL–DA	SCPL	PDMS-containing scaffolds mineralized in 1X SBF and presented accelerated degradation rates.
	Beltran, 2023[108]	PMHS–DMA	PCL–DA	SCPL	PMHS-containing scaffolds had a faster onset of acellular mineralization in SBF, and expedited acceleration profiles compared to analogous PDMS scaffolds.

polymer. In some cases, bioactivity is demonstrated in the absence of bioactive fillers. For instance, collagen has been blended with polyesters to form electrospun scaffolds,[116] including for bone regeneration per Jose *et al.*[100] Wang *et al.* combined gelatin with PCL to produce scaffolds with hierarchal morphological structures using melt electrospinning writing (MEW) and solution electrospinning (SE).[101] Amiryaghoubi *et al.* introduced chitosan to PCL/polyurethane (PU) to form scaffolds *via* freeze-drying.[102] Ren *et al.* prepared PCL scaffolds *via* MEW and was subsequently impregnated with fibrin/alginate (FA).[103] Jang *et al.* reported PCL/hyaluronic acid microspheres that were embedding into a tissue defect using an *in situ* gelling alginate hydrogel.[104]

Inspired by bioactive silicates, we have utilized silicon-based synthetic polymers as bioactive additives to form bone tissue scaffolds. While poly(ethylene glycol) (PEG) hydrogels have been evaluated for bone regeneration, they lack innate bioactivity.[117] Thus, *star*-polydimethylsiloxane methacrylate ($PDMS_{star}$–MA) and PEG–diacrylate (PEG–DA) macromers were combined to form templated PDMS–PEG hydrogels that exhibited acellular mineralization when exposed to SBF, as well as enhanced osteogenesis of cultured hBMSCs.[105] Greater bioactivity was observed for phosphonated-siloxane PEG hydrogels prepared with a poly(diethyl(2-(propylthio)-ethyl)phosphonate methylsiloxane)–diacrylate (PPMS–DA) macromer.[106] Finally, we sought to induce bioactivity to our previously reported PCL SMP scaffolds.[39] In the first study, PDMS–dimethacrylate (DMA) was combined with PCL–DA at varying wt% ratios (90 : 10, 75 : 25, and 60 : 40), giving rise to PCL–PDMS scaffolds.[107] These maintained shape memory behavior, but displayed acellular mineralization with SBF exposure, as well as enhanced degradation rates due to phase separation effects. In a subsequent study, towards the goal of enhancing bioactivity, polymethylhydrosiloxane–dimethacrylate (PMHS–DMA) was utilized to form analogous PCL–PMHS scaffolds.[108] The increased hydrophilicity of PMHS *versus* PDMS, stemming from the capacity of silane (Si–H) groups to form dihydrogen bonding with hydroxyl (–OH) groups of water, was expected to better parallel hydrophilic bioactive silicates. Indeed, PCL–PMHS scaffolds exhibited enhanced rates of HAp mineralization, as well as *in vitro* degradation rates. However, incorporation of a PEG-tethered cell adhesive peptide to PCL–PMHS scaffolds resulted in less presentation at the surface, reducing cellular adhesion.

For the future development of bioactive materials, the combination of high throughput screening (HTS)[118,119] along with artificial intelligence (AI),[120] specifically machine learning (ML),[121] has great potential. ML used to analyze data from HTS assays can be critical in predicting properties of regenerative scaffolds, with different material combinations. For HTS and ML to be effective toward generating and predicting attributes of bioactive scaffolds, there must be standardized protocols for testing, which is currently lacking.[122] In addition to selecting optimal material combinations, AI can be helpful in determining suitable 3D printing fabrication techniques and scaffold structure depending on the patient and location of the bone defect. Integrating AI with computer-aided design (CAD) to 3D print patient-specific scaffolds, especially with complex geometries, can reduce the time to generate scaffold structures and facilitate the selection of scaffold parameters (*e.g.*, pore size, percent porosity, strut size) to mimic the adjacent trabecular or cortical bone. For example, after an imaging modality (*e.g.*, CT scan) is used to identify the exact geometry of the defect, the AI integrated CAD system could generate a 3D scaffold that perfectly fits into the bone defect to enable proper osseointegration and angiogenesis through the scaffold.[123] Furthermore, the use of AI techniques to determine optimal scaffold parameters during fabrication can pave the way for more thorough *in vitro* and *in vivo* assessments of the most promising scaffold compositions.

3. Assessment of scaffold of bioactivity

A number of analyses have been used to assess scaffold bioactivity, namely *via* acellular HAp formation, *in vitro* cellular behavior, and *in vivo* bone formation (Fig. 4). Assessment of acellular bioactivity should also consider scaffold sterilization and any pre-treatments (*e.g.*, pre-wetting with ethanol graded baths) to be used for subsequent *in vitro* cell culture or *in vivo* assessment.

3.1. *In vitro* (acellular) assessment of scaffold bioactivity

Immersion of scaffolds to induce mineralization. SBF has been widely adopted to measure bioactivity of materials, including per ISO 23317.[124] Exposure to SBF, which is acellular and protein-free, is frequently utilized to confirm scaffold bioactivity in terms of HAp formation.[14,44,125] Developed by Kokubo in 1991,[126] SBF mimics the inorganic composition of human plasma (*e.g.*, Mg^{2+}, Ca^{2+}, Na^{+}, and K^{+}) with a physiological pH ($\sim$7.4), and is used at body temperature ($\sim$37 °C). Kokubo *et al.* suggested the SBF volume (in mL) be greater than 1/10 the surface area of a porous material (in mm^2).[44] As a means to accelerate mineralization, SBF of higher concentrations have been utilized.[85] However, highly concentrated SBF solutions can produce uneven, localized precipitation onto surfaces, and also exhibit spontaneous precipitation. This may be somewhat mitigated by increasing the temperature[127] or decreasing pH of concentrated SBF solution.[128] Due to the labor-intensive preparation of SBF, alternatives have been explored. Dulbecco's modified Eagle medium (DMEM), a commercially available cell culture medium, possesses ion concentrations similar to that of human blood plasma.[129] α-TCP, β-TCP, and HAp were each incubated in DMEM (37 °C, 5% CO_2) for 4 days, leading to CaP precipitate on these surfaces. However, it was noted that the presence of serum can decrease the rate of precipitation.

Scanning electron microscopy (SEM)/energy-dispersive X-ray spectroscopy (EDS). SEM/EDS may be used in conjunction to evaluate the mineralized surface of bioactive scaffolds, including after immersion in SBF. SEM is frequently utilized to provide images of scaffold morphology and microstructure.[130] Coupling with EDS affords determination of elemental

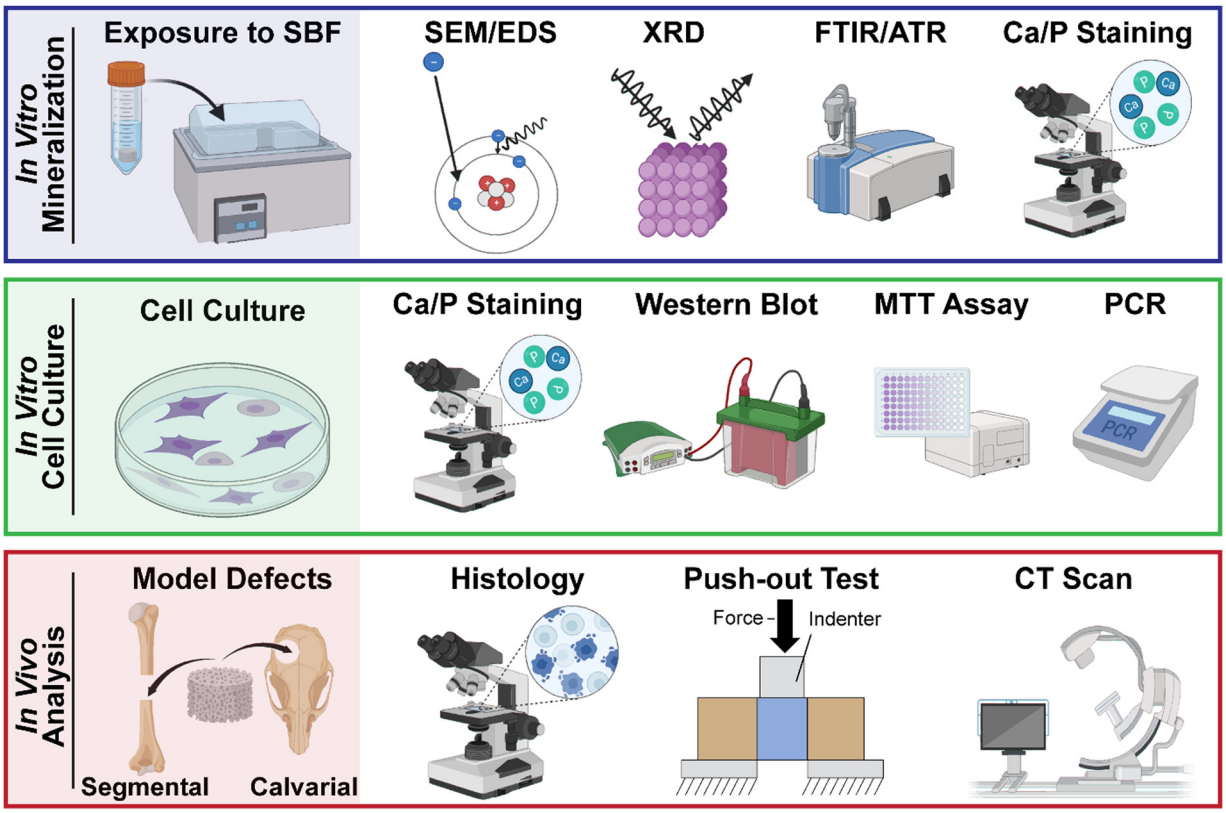

Fig. 4 Generalized methods for assessing scaffold bioactivity: (top) acellular mineralization *via* exposure to SBF, characterization of HAp mineralization, (middle) cell culture, and (bottom) *in vivo* analyses using bone defect models.

composition of the surface.[131] Briefly, when the surface is penetrated by the electron beam, element-specific X-rays are emitted and can be quantified by the spectrometer. SEM/EDS can thus determine the Ca to P molar ratio of a surface, which is ~1.67 in the case of HAp.[132]

X-ray diffraction (XRD). Another tool used to confirm HAp mineralization on scaffolds is XRD based on the characteristic diffraction signature.[133–136] Briefly, incident X-rays irradiate the surface and the intensities and scattering angles of the emitted X-rays are measured.[137] XRD can determine HAp phase composition, degree of crystallinity, and crystallite size.[134,138,139]

Vibrational spectroscopy. Attenuated total reflectance-Fourier transform infrared (ATR-FTIR) spectroscopy is also commonly used to evaluate HAp mineralization.[140,141] Briefly, molecular functional groups are revealed by nature of their distinct IR absorption band.[142] The ATR mode configuration acquires molecular vibrations through a reduced path length of the probing IR beam, allowing evaluation of the surface to a depth of a few micrometers. ATR-FTIR can be used to identify PO_4^{3-} [~560 and 600 cm^{-1} and ~1000–1100 cm^{-1}], CO_3^{2-} [between ~1460 and ~1530 cm^{-1}], and OH^- [~3570 cm^{-1}] groups present in HAp.[138,143] HAp formation, size, and distribution may be assessed with FTIR imaging *via* micro-ATR-IR.[144] Raman spectroscopy has also been used to evaluate HAp deposits onto scaffolds *via* the inelastic scattering of light, and water produces less interference *versus* IR spectroscopy.[145,146]

Staining. Staining techniques can be used to evaluate acellular HAp mineralization of bioactive scaffolds. These methods generally involve incubation of the mineralized specimen in an aqueous staining solution, followed by fluorescent imaging and analysis (*e.g.*, with ImageJ software) to yield mineral intensity or mineralized area (% coverage).[147,148] While advantageously rapid, most stains lack specificity to HAp mineral deposits *versus* calcium- and phosphate-containing deposits and so cannot be used alone to identify HAp.

Alizarin red S, [3,4-dihydroxy-9,10-dioxo-9,10-dihydroanthracene-2-sulfonic acid; $C_{14}H_7NaO_7S$; "AzHNa"] is a water-soluble sodium salt of Alizarin sulfonic acid that undergoes a reaction with HAp, described as follows:[149]

$$Ca_{10}(PO_4)_6(OH)_2 + 10AzHNa \rightarrow 10CaAz\downarrow + HPO_4^{2-} + 2H_2PO_4^- + 10Na^+ + 2H_2O$$

The red/orange colored precipitate can be quantified, permitting the relative extent of HAp mineralization to be compared across specimens. Per Gregory *et al.*, the precipitate can be removed *via* acetic acid extraction, neutralized with ammonium hydroxide, and absorbance intensity evaluated by a scanning spectrometer at 405 nm.[150] Alizarin red S staining is not specific to HAp, and will likewise produce such deposits from other sources of Ca^{2+} ions.[151]

Von Kossa staining may also be used to evaluate HAp mineralization on scaffolds. Von Kossa staining utilizes a silver

nitrate solution to transform calcium phosphate salts to silver phosphate salts, described as follows:[152]

$$Ca_3(PO_4)_2 + 6AgNO_3 \rightarrow 3Ca(NO_3)_2 + \downarrow 2Ag_3PO_4$$

The grey/black precipitate can be quantified to afford comparison of scaffold specimen HAp mineralization. However, this stain is not specific to phosphates of HAp, and cannot be used to provide absolute identification of HAp.[153]

Other dyes that can stain HAp mineral deposits on scaffolds include xylenol orange and calcein blue.[154,155] Xylenol orange [3,3′-bis[*N*,*N*-bis(carboxymethyl)amino-methyl]-*o*-cresolsulf-onephthalein tetrasodium salt; $C_{31}H_{28}N_2Na_4O_{13}S$] forms orange, fluorescent complexes with divalent metal ions (*e.g.*, Ca^{2+}).[156] Calcein blue [4-methylumbelliferone-8-methyliminodiacetic acid] also binds to calcium to afford blue staining of the mineral.[157]

The OsteoImage™ mineralization assay (Lonza) is based on a fluorescent stain that is advantageously specific to HAp mineralization. Thus, OsteoImage™ has been used to stain HAp deposits formed *via* acellular mineralization[158,159] as well as following cell culture.[160–162]

3.2. *In vitro (cellular)* culture to assess scaffold bioactivity

The bioactivity of scaffolds may also be assessed *via* cell culture.[163] A variety of cell sources have been implemented, namely stem cells such as bone marrow mesenchymal stems cells (BMSCs), adipose-derived MSCs (ASCs), perivascular stem cells, and induced pluripotent stem cells (iPSCs).[164] Such osteoprogenitor cells undergo osteogenic differentiation into osteoblasts, osteoclasts, and osteocytes, all cells found in native bone tissue.[165] Originating from the bone marrow, BMSCs have been particularly utilized in bone regeneration strategies.[166] Biomolecules, such as the fibronectin-derived peptide sequence Arg–Gly–Asp–Ser (RGDS), are often incorporated into the scaffold to direct or support desired stem cell adhesion, spreading, and differentiation.[91] Exogenous (external) growth factors, particularly BMP-2, have also been incorporated into scaffolds to accelerate osteogenesis, although these strategies often risk off-target effects *in vivo*.[32] A wide range of methods have been used for biomolecule incorporation, as a single method of biomolecule incorporation is not necessarily universally effective for all scaffold types. For instance, phase separation within the scaffold can alter incorporated biomolecule surface presentation.[108] Fluorescent imaging can be used to confirm the quality of cellular adhesion and spreading, whereby fixed cells are stained with phalloidin (cellular actin cytoskeleton) and DAPI [4′,6-diamidino-2-phenylindole] (cell nuclei).[167] Prior to the aforementioned analyses, the cytocompatibility of the scaffold should be confirmed using a variety of assays (*e.g.*, MTT assay,[168] or lactate dehydrogenase [LDH] assay[169]).

Scaffolds that demonstrate cytocompatibility and the capacity to support cell adhesion and spreading, are often then evaluated for their capacity to support the osteogenic differentiation of adherent stem cells. In these studies, osteogenic medium – typically prepared by supplementing a conventional medium with some combination of L-ascorbic acid, β-glycerophosphate, and dexamethasone – may be utilized to mimic the osteogenic milieu present in bone.[170,171] During osteogenesis, stem cells cultured on bioactive scaffolds will produce HAp deposits, the extent to which can be evaluated using histological methods with some of the previously noted stains (*e.g.*, Alizarin red S and von Kossa[150,172]). The expression of the numerous osteogenic markers involved in osteogenesis,[171] and methods for assessment have been recently reviewed by Le *et al.*[173] Briefly, following a defined period of culture, the scaffold homogenates may be subjected to a variety of analyses to detect the expression of mRNA levels of genes (*via* polymerase chain reaction [PCR]) or expression of proteins (*via* immunofluorescence staining, western blot, and ELISA assays). Multiple osteogenic markers are typically evaluated as each gives insight into specific aspects of osteogenesis, including stages of progression. These include transcription factors (*e.g.*, RUNX2, Osterix, Msx2), extracellular matrix proteins[174] (*e.g.* secreted protein acidic and rich cysteine [SPARC], osteopontin [OPN], osteocalcin, collagen 1 α1 chain [COL1A1]), and secreted growth factors[175] (*e.g.*, vascular endothelial growth factor [VEGF],[176] BMP-2,[177] and BMP-4[178]). ALP, an early marker of osteoblast differentiation, is often quantified as an indicator of scaffold bioactivity.[179,180] Expression of ''off-target'' markers can also be assessed to delineate the specificity of scaffold bioactivity for osteogenesis. Off-target evaluation often includes assessment of markers for chondrogenic (*e.g.*, SRY-box transcription factor 9 [SOX9] and collagen 2 α1 chain [COL2A1]) and adipogenic (*e.g.*, CCAAT/enhancer binding protein [α-C/EBP-α], and adipocyte fatty acid binding protein [AFABP]) differentiation.

3.3. *In vivo and ex vivo* methods to assess scaffold bioactivity

A number of *in vivo* and *ex vivo* models of bone repair are available for the assessment of bioactive scaffolds.[181] Animal species that have been utilized include rodent, rabbit, dog, sheep, goat, and pig, with each presenting unique advantages and disadvantages.[182] Bone defects are frequently created in calvariae [as confined defects], or in ulnae, tibiae, and femurs [as segmental defects]. The minimum size for a critical defect, wherein spontaneous healing does not occur over a long duration, must be considered.[183,184] However, non-critically sized calvarial defects, permitting two rather than one defect per animal, have been used to assess scaffold osseointegration and neotissue infiltration at the perimeter.[39] This approach exemplifies a potential way to commit to the 3Rs (reduce, replace, refine) principle of humane animal research.[185] Recently, models have also been created to assess osteoporotic defect healing,[186,187] and attention has been given to sex-based differences in bone defect healing.[188] Several methods to detect *in vivo* mineralization of scaffold treated defects have been commonly employed as highlighted below. Tissue preservation is required for most *ex vivo* analyses, and includes methods such as slow freezing, vitrification, hypothermic preservation, and cryopreservation.[189]

***In vivo* analyses.** Numerous methods exist for non-invasive, longitudinal monitoring of scaffold-induced bone

regeneration, including bone mineral density (BMD).[190,191] Micro-computed tomography (micro-CT) is perhaps the most widely utilized, given its relative low cost and efficacy.[192,193] Having a spatial resolution of 50–1 μm,[194] micro-CT affords 3D evaluation of bone ingrowth and volumetric changes. Micro-CT can also be used to determine BMD (mg HAp cm^{-3}).[195] Positron emission tomography (PET) can be used to evaluate longitudinal bone formation using γ-ray emitting tracers, such as a sodium fluoride ([^{18}F]–NaF) that forms fluoroapatite with HAp of new bone tissue.[196] Bone regeneration can also be monitored by single-photon emission computed tomography (SPECT) employing positron-emitting tracers, such as ^{99m}technetium [^{99m}Tc-labelled diphosphonates] that are absorbed by HAp.[197] Dual-modality, integrated micro-CT/PET[198,199] and micro-CT/SPECT[199] images have been used to assess scaffold-induced bone regeneration. Dual-energy X-ray absorptiometry (DEXA) may also be used to assess BMD.[200–202] Other methods of non-invasive monitoring have been employed to avoid potential tissue damage associated with X-rays. Magnetic resonance imaging (MRI) based on semi-quantitative methods may be employed to overcome low sensitivity to bone.[203] For instance, Ribot *et al.* developed a 3D anatomic and perfusion MRI protocol to observe scaffold-induced healing of femoral defects in rats, including mineralization and neovascularization.[204] Ultrasound imaging, while limited by depth of penetration, may be used to quantify bone regeneration.[205] Optical fluorescence imaging (*e.g.*, IVIS) can be performed on fluorescently-labelled scaffolds to monitor resorption *in vivo*.[201]

***Ex vivo* analyses.** Endpoint tissue specimens harvested from experimental models, as well as tissue culture specimens, are frequently evaluated with the aforementioned *in vivo* methods. Micro-CT is widely used to view morphological features and HAp mineral deposits, wherein longer scan times are permitted for improved spatial resolution.[193] Environmental SEM is also useful as it retains the natural state of the specimen by excluding the need for high vacuum conditions, as well as specimens that are clean, dry, and electrically conductive.[206] Other examples demonstrate the use of *ex vivo* MRI,[207] DEXA,[208] and ultrasound[209] in the evaluation of endpoint tissue specimens. Raman spectroscopy is also useful to evaluate the chemical properties of regenerated bone tissue at the nanoscale, including the degree of mineralization.[210,211]

Histological and histomorphometric analyses. Histological and histomorphometric analyses of regenerated, mineralized bone tissue is crucial in assessing the bioactivity of scaffolds. Bone histomorphometry provides quantitative evaluation through the use of digitized histological images,[212,213] using various image analysis platforms.[214,215] Typically, harvested specimens are sequentially fixed, decalcified, dehydrated, embedded (*e.g.*, in paraffin or PMMA), and sectioned. A variety of stains are available for these analyses, including some mentioned previously to detect acellular mineralization of scaffolds. Hematoxylin & eosin (H&E) staining – which stains cell nuclei a dark blue/purple color and basic proteins in the ECM a pink/orange color[216,217] – is useful to identify woven bone, an early stage of bone development characterized by random collagen matrix deposition.[39,218] Masson's trichrome staining employs acid–base chemistry by using 3 dyes to selectively stain tissue components.[219] When staining for bone regeneration, new bone, collagen, and osteoids are stained blue, while mature bone is stained red.[220] Von Kossa staining can also be used to differentiate mineralized [stained black] *versus* unmineralized [stained red] bone matrix produced by bioactive scaffolds.[213]

Mechanical testing. A variety of biomechanical tests are utilized to evaluate the efficacy of scaffolds to promote bone regeneration in experimental models.[221,222] In macroscopic assessments, harvested constructs are frequently subjected to quasi-static tests wherein stress or strain is applied in different modes (*e.g.*, compression, tension, bending, torsion, and shear). Bulk modulus, strength, and toughness values can then be determined. In some cases, standards are applied such as ISO 604[223–225] and ISO 5833.[226,227] Push-out tests are also frequently employed to give insight into scaffold osteointegration with surrounding tissues, and efforts continue to be made to refine best practices.[228] Microscopic biomechanical analyses are also utilized to give insight into nanoscale mechanical properties.[222] Nanoindentation can be utilized to measure enhanced local hardness imparted by mineralized bone tissue.[211] Atomic force microscopy (AFM), using contact or tapping modes, can be used to reveal nanoscale features (*e.g.*, collagen fibrils and HAp crystals), while the nanoindentation mode is useful for nanomechanical modulus mapping.[229–231] Sub-resonance AFM (*e.g.*, PeakForce Tapping mode) has also been developed for nanomechanical mapping[232] and was used by Zhou *et al.* to evaluate bone tissue submerged in an aqueous environment.[233] It was also shown that micro-CT has also been coupled with mechanical testing to measure contact area and 3D full-field strain in bone/dental implant constructs;[234] such a method could likewise be highly informative to the assessment of bioactive scaffolds.

4. Conclusions

Bioactive scaffolds remain a contemporary approach to bone regenerative engineering. Emerging in recent years are an array of methods to induce bioactivity to polymeric scaffolds that utilize bioceramic fillers, coatings and surface treatments, and additives. Bioactive composite scaffolds continue to be formed with traditional bioceramic fillers (*e.g.*, DBM and BGs), including combinations of two or more types. Newer bioceramics have also emerged (*e.g.*, LAPONITE® and eggshell microparticles). Bioactive coatings applied to scaffolds include deposited bioceramics, bioceramics embedded in a polymer matrix, and polymer-only types. Surface treatments such as plasma treatment, PECVD, and iCVD have also been leveraged to induce bioactivity. Finally, bioactive additives have been combined with 'bioinert' polymers to form bioactive scaffolds. Such additives include primarily certain natural polymers (*e.g.*, chitosan and collagen), as well as silicon- and phosphonated/silicon-based synthetic polymers. Overall, these methods yield

bioactivity throughout the scaffold (*via* fillers and additives) or at the surface of the scaffold (*via* coatings and surface treatments). For the former types, bulk properties (*e.g.*, stiffness and degradation) are impacted which may or may not be desirable. With surface modification, bulk properties are retained, but bioactivity can be expected to be diminished when the surface is lost. High throughput screening and machine learning will be critical for efficient and successful future development of bioactive scaffolds, but necessitates standardized characterization methods. AI integrated CAD also has potential to play a pivotal role in the treatment of patient-specific complex bone defects. A plethora of *in vitro* (acellular and cellular), *in vivo*, and *ex vivo* methods exist to evaluate scaffold mineralization and other aspects of bone regeneration. Perhaps the most common initial assessment of scaffold bioactivity is the capacity to undergo HAp mineralization when exposed to SBF. HAp can be subsequently assessed with numerous methods (*e.g.*, imaging, spectroscopy, and staining). Mineralization by cultured cells, particularly MSCs, as well as evaluation of other markers of osteogenesis is also commonly used to assess scaffold bioactivity. Such analyses typically rely on staining techniques and other assays. *In vivo* models of bone repair afford an opportunity to assess scaffold bioactivity in a physiological environment. Several assessment methods (*e.g.*, PET, SPECT, and MRI) afford longitudinal monitoring of mineralization and tissue regeneration, with micro-CT being the most frequently employed. Harvested endpoint tissue specimens typically undergo histological and histomorphometric analyses, and biomechanical assessments are also valuable. While recent studies highlight the breadth of methods to prepare and assess bioactive scaffolds, several primary challenges remain for bioactive scaffold-based approaches to displace the clinical use of standard biological and alloplastic grafting. Overall, comparison of scaffold bioactivity in the literature is difficult. Studies employ different analyses (*e.g.*, methods, test conditions, and selected time points) to assess bioactivity both *in vitro* and *in vivo*. Thus, standardized methods would be extremely useful to the field. Controls that could be uniformly included along with experimental scaffolds would also be beneficial to studies, but are currently lacking.[235] Explant cultures (a.k.a. organ or *ex vivo* cultures), wherein explanted tissue-scaffold constructs are maintained *in vitro* and often with applied mechanical loading, may provide a valuable intermediate step between *in vitro* cell culture and *in vivo* experimental models.[236] Despite these challenges, bioactive scaffolds hold tremendous promise in the treatment of bone defects.

Author contributions

Brandon Nitschke: writing – conceptualization, visualization, writing – original draft, writing – review & editing; Felipe Beltran: conceptualization, writing – original draft, writing – review & editing; Mariah Hahn: writing – review & editing; Melissa Grunlan: writing – original draft, writing – review & editing.

Conflicts of interest

There are no conflicts to declare.

Acknowledgements

Funding from NIH/NIDCR (1R01DE025886-01A1) is gratefully acknowledged.

References

1 R. Florencio-Silva, G. R. Sasso, E. Sasso-Cerri, M. J. Simões and P. S. Cerri, *Biomed. Res. Int.*, 2015, **2015**, 421746.
2 X. Lin, S. Patil, Y.-G. Gao and A. Qian, *Front. Pharmacol.*, 2020, **11**, 757.
3 E. Roddy, M. R. DeBaun, A. Daoud-Gray, Y. P. Yang and M. J. Gardner, *Eur. J. Orthop. Surg. Traumatol.*, 2018, **28**, 351–362.
4 W. Wang and K. W. K. Yeung, *Bioactive Mater.*, 2017, **2**, 224–247.
5 R. Amid, A. Kheiri, L. Kheiri, M. Kadkhodazadeh and M. Ekhlasmandkermani, *Int. Union Biochem. Mol. Biol.*, 2020, **68**, 1432–1452.
6 H. J. Haugen, S. P. Lyngstadaas, F. Rossi and G. Perale, *J. Clin. Periodontol.*, 2019, **46**(Suppl. 21), 92–102.
7 H. Zhang, L. Yang, X.-G. Yang, F. Wang, J.-T. Feng, K.-C. Hua, Q. Li and Y.-C. Hu, *Orthopaedic Surg.*, 2019, **11**, 725–737.
8 J. R. Jones, D. S. Brauer, L. Hupa and D. C. Greenspan, *Int. J. Appl. Glass Sci.*, 2016, **7**, 423–442.
9 J. R. Jones, *Acta Biomater.*, 2013, **9**, 4457–4486.
10 Z. Bal, T. Kaito, F. Korkusuz and H. Yoshikawa, *Emergent Mater.*, 2020, **3**, 521–544.
11 N. Ramesh, S. C. Moratti and G. J. Dias, *J. Biomed. Mater. Res., Part B*, 2018, **106**, 2046–2057.
12 V. S. Kattimani, S. Kondaka and K. P. Lingamaneni, *Bone Tissue Regener. Insights*, 2016, **7**, 36138.
13 H. Lu, Y. Zhou, Y. Ma, L. Xiao, W. Ji, Y. Zhang and X. Wang, *Front. Mater.*, 2021, **15**, 698915.
14 M. Bohner, B. L. G. Santoni and N. N. Döbelin, *Acta Biomater.*, 2020, **113**, 23–41.
15 A. W. Barone, S. Andreana and R. Dziak, *Med. Res. Arch.*, 2020, **8**, DOI: **10.18103/mra.v8i11.2283**.
16 D. Liu, C. Cui, W. Chen, J. Shi, B. Li and S. Chen, *J. Funct. Biomater.*, 2023, **14**, 134.
17 A.-M. Yousefi, *J. Appl. Biomater. Funct. Mater.*, 2019, **17**, 2280800019872594.
18 K. A. Cole, G. A. Funk, M. N. Rahaman and T. E. McIff, *J. Biomed. Mater. Res., Part B*, 2020, **108**, 1580–1591.
19 M. R. Senra and M. d F. V. Marques, *J. Compos. Sci.*, 2020, **4**, 191.
20 M. Alizadeh-Osgouei, Y. Li and C. Wen, *Bioactive Mater.*, 2019, **4**, 23–26.
21 L. Guo, Z. Lian, L. Yang, W. Du, T. Yu, H. Tang, C. Li and H. Qiu, *J. Controlled Release*, 2021, **338**, 571–582.

22 M. Filippi, G. Born, M. Chaaban and A. Scherberich, *Front. Bioeng. Biotechnol.*, 2020, **8**, 474.
23 C. Sun, J. Kang, C. Yang, J. Zheng, Y. Su, E. Dong, Y. Liu, S. Yao, C. Shi and H. Pang, *Biomater. Transl.*, 2022, **3**, 116.
24 B. I. Oladapo, S. A. Zahedi, S. O. Ismail and F. T. Omigbodum, *Colloids Surf., B*, 2021, **203**, 111726.
25 H. Wang, P. Chen, Z. Shu, A. Chen, J. Su, H. Wu, Z. Chen, L. Yang, C. Yan and Y. Shi, *Compos. Sci. Technol.*, 2023, **231**, 109805.
26 A. S. Mao and D. J. Mooney, *Proc. Natl. Acad. Sci. U. S. A.*, 2015, **112**, 14452–14459.
27 G. L. Koons, M. Diba and A. G. Mikos, *Nat. Rev. Mater.*, 2020, **5**, 584–603.
28 K. S. Ogueri, T. Jafari, J. L. E. Ivirico and C. T. Laurencin, *Regener. Eng. Transl. Med.*, 2019, **5**, 128–154.
29 T. Albrektsson and C. Johansson, *Eur. Spine J.*, 2001, **10**(Suppl. 2), S96–S101.
30 Y. Du, J. L. Guo, J. Wang, A. G. Mikos and S. Zhang, *Biomaterials*, 2019, **218**, 119334.
31 X. Yu, X. Tang, S. V. Gohil and C. T. Laurencin, *Adv. Healthcare Mater.*, 2015, **4**, 1268–1285.
32 D. Halloran, H. W. Durbano and A. Nohe, *J. Dev. Biol.*, 2020, **8**, 19.
33 E. Alsberg, E. E. Hill and D. J. Mooney, *Crit. Rev. Oral Biol. Med.*, 2001, **12**, 64–75.
34 T. Blokhuis and J. C. Arts, *Injury*, 2011, **42**, S26–S29.
35 M. N. Collins, G. Ren, K. Young, S. Pina, R. L. Reis and J. M. Oliveira, *Adv. Funct. Mater.*, 2021, **31**, 2010609.
36 B. Chang, N. Ahuja, C. Ma and X. Liu, *Mater. Sci. Eng., R*, 2017, **111**, 1–26.
37 M. Mirkhalaf, Y. Men, R. Wang, Y. No and H. Zreiqat, *Acta Biomater.*, 2023, **156**, 110–124.
38 M. Ly, S. Spinelli, S. Hays and D. Zhu, *Eng. Regen.*, 2022, **3**, 41–52.
39 M. R. Pfau, F. O. Beltran, L. N. Woodard, L. K. Dobson, S. B. Gasson, A. B. Robbins, Z. T. Lawson, W. B. Saunders, M. R. Moreno and M. A. Grunlan, *Acta Biomater.*, 2021, **136**, 233–242.
40 D. M. Yunos, O. Bretcan and A. R. Boccaccini, *J. Mater. Sci.*, 2008, **43**, 4433–4442.
41 F. Baino, G. Novajra and C. Vitale-Brovarone, *Front. Bioeng. Biotechnol.*, 2015, **3**, 202.
42 G. Turnbull, J. Clarke, F. Picard, P. Riches, L. Jia, F. Han, B. Li and W. Shu, *Bioactive Mater.*, 2018, **3**, 278–314.
43 L. L. Hench, N. Roki and M. B. Fenn, *J. Mol. Struct.*, 2014, **1073**, 24–30.
44 T. Kokubo and H. Taakadama, *Biomaterials*, 2006, **27**, 2907–2915.
45 H.-M. Kim, T. Himeno, T. Kokubo and T. Nakamura, *Biomaterials*, 2005, **26**, 4366–4373.
46 Q. Zhang, J. Zhou, P. Zhi, L. Liu, C. Liu, A. Fang and Q. Zhang, *Med. Nov. Technol.*, 2023, **17**, 10025.
47 C. Shuai, W. Yang, P. Feng, S. Peng and H. Pan, *Bioactive Mater.*, 2021, **6**, 490–502.
48 S. Xu, J. Liu, L. Zhang, F. Yang, P. Tang and D. Wu, *J. Mater. Chem. B*, 2017, **5**, 6110–6118.
49 W.-X. Cheng, Y.-Z. Liu, X.-B. Meng, Z.-T. Zheng, L.-L. Li, L.-Q. Ke, L. Ling, C.-S. Huang, G.-Y. Zhu, H.-D. Pan, L. Qing, X.-L. Wang and P. Zhang, *J. Orthop. Translat.*, 2021, **31**, 41–51.
50 E. Nyberg, A. Rindone, A. Dorafshar and W. L. Grayson, *Tissue Eng., Part A*, 2017, **23**, 503–514.
51 C. Shuai, L. Yu, P. Feng, S. Peng, H. Pan and X. Bai, *J. Mater. Chem. B*, 2022, **10**, 214–223.
52 S. Sultan, N. Thomas, M. Varghese, Y. Dalvi, S. Joy, S. Hall and A. P. Mathew, *Molecules*, 2022, **27**, 7214.
53 B. M. Nitschke, A. E. Konz, E. A. Butchko, M. N. Wahby and M. A. Grunlan, 2023 MRS Fall Meeting, 2023.
54 T. Distler, N. Fournier, A. Grünewald, C. Polley, H. Seitz, R. Detsch and A. R. Boccaccini, *Front. Bioeng. Biotechnol.*, 2020, **8**, 552.
55 M. H. Monfared, F. E. Ranjbar, M. Torbati, S. A. Poursamar, N. Lotfibakhshaiesh, J. Ai, S. Ebrahimi-Barough and M. Azami, *J. Non-Cryst. Solids*, 2022, **593**, 121769.
56 J. Han, J. Wu, X. Xiang, L. Xie, R. Chen, L. Li, K. Ma, Q. Sun, R. Yang and T. Huang, *Mater. Des.*, 2023, **225**, 111543.
57 F. Westhauser, F. Hohenbild, M. Arango-Ospina, S. I. Schmitz, S. Wilkesmann, L. Hupa, A. Moghaddam and A. R. Boccaccini, *Int. J. Mol. Sci.*, 2020, **21**, 1639.
58 X. Du, D. Wei, L. Huang, M. Zhu, Y. Zhang and Y. Zhu, *Mater. Sci. Eng., C*, 2019, **103**, 109731.
59 X. Qi, P. Pei, M. Zhu, X. Du, C. Xin, S. Zhao, X. Li and Y. Zhu, *Sci. Rep.*, 2017, **7**, 42556.
60 J. K. Carrow, A. Di Luca, A. Dolatshahi-Pirouz, L. Moroni and A. K. Gaharwar, *Regener. Biomater.*, 2019, **6**, 29–37.
61 X. Wu, O. Gauntlett, T. Zhang, S. Suvarnapathaki, C. McCarthy, B. Wu and G. Camci-Unal, *ACS Appl. Mater. Interfaces*, 2021, **13**, 60921–60932.
62 B. Huang, C. Vyas, J. J. Byun, M. El-Newehy, Z. Huang and P. Bártolo, *Mater. Sci. Eng., C*, 2020, **108**, 110374.
63 D. Zhang, O. J. George, K. M. Petersen, A. C. Jimenez-Vergara, M. S. Hahn and M. A. Grunlan, *Acta Biomater.*, 2014, **10**, 4597–4605.
64 L. N. Woodard, K. T. Kmetz, A. A. Roth, V. M. Page and M. A. Grunlan, *Biomacromolecules*, 2017, **18**, 4075–4083.
65 D. A. Oluwatosin, K. El Mabrouk and M. Bricha, *J. Mater. Chem. B*, 2023, **11**, 955–973.
66 J. Hatton, G. R. Davis, A.-H. I. Mourad, N. Cherupurakal, R. G. Hill and S. Mohsin, *J. Funct. Biomater.*, 2019, **10**, 15.
67 M. Schumacher, P. Habibovic and S. van Rijt, *Bioact. Mater.*, 2020, **6**, 1921–1931.
68 M. V. Thomas and D. A. Puleo, *J. Biomed. Mater. Res., Part B*, 2008, **88B**, 597–610.
69 Y. Zhao, Z. Zhang, Z. Pan and Y. Liu, *Exploration*, 2021, **1**, 20210089.
70 M. Du, J. Chen, K. Liu, H. Xing and C. Song, *Composites, Part B*, 2021, **215**, 108790.
71 A. K. Gaharwar, S. M. Mihaila, A. Swami, A. Patel, S. Sant, R. L. Reis, A. P. Marques, M. E. Gomes and A. Khademhosseini, *Adv. Mater.*, 2013, **25**, 3329–3336.

72 J. K. Carrow, L. M. Cross, R. W. Reese, M. K. Jaiswal, C. A. Gregory, R. Kaunas, I. Singh and A. K. Gaharwar, *Proc. Natl. Acad. Sci. U. S. A.*, 2018, **115**, E3905–E3913.
73 T. L. Shi, Y. F. Zhang, M. X. Yao, C. Li, H. C. Wang, C. Ren, J. S. Bai, X. Cui and W. Chen, *Biomater. Transl.*, 2023, **4**, 131.
74 T. Zheng, Y. Huang, X. Zhang, Q. Cai, X. Deng and X. Yang, *J. Mater. Chem. B*, 2020, **8**, 10221–10256.
75 K. A. Kravanja and M. Finšgar, *Mater. Des.*, 2022, **217**, 110653.
76 N. R. Richbourg, N. A. Peppas and V. I. Sikavitsas, *J. Tissue Eng. Regener. Med.*, 2019, **13**, 1275–1293.
77 H. F. Pereira, I. F. Cengiz, F. S. Silva, R. L. Reis and J. M. Oliveira, *J. Mater. Sci.: Mater. Med.*, 2020, **31**, 27.
78 N. Fazeli, E. Arefian, S. Irani, A. Ardeshirylajimi and E. Seyedjafari, *Sci. Rep.*, 2023, **13**, 12145.
79 Y. Zhang, J.-I. Jo, L. Chen, S. Hontsu and Y. Hashimoto, *Int. J. Mol. Sci.*, 2022, **23**, 9048.
80 T.-T. Li, L. Ling, M.-C. Lin, Q. Jiang, Q. Lin, J.-H. Lin and C.-W. Lou, *Nanomaterials*, 2019, **9**, 679.
81 S. K. L. Levengood and M. Zhang, *J. Mater. Chem. B*, 2014, **2**, 3161–3184.
82 M. Shaltooki, G. Dini and M. Mehdikhani, *Mater. Sci. Eng., C*, 2019, **105**, 110138.
83 L. Fan, Y. Ren, S. Emmert, I. Vuckovic, S. Stojanovic, S. Najman, R. Schnettler, M. Barbeck, K. Schenke-Layland and X. Xiong, *Int. J. Mol. Sci.*, 2023, **24**, 3744.
84 F. Tabatabaei, A. Gelin, M. Rasoulianboroujeni and L. Tayebi, *Colloids Surf., B*, 2022, **217**, 112670.
85 B. Yilmaz, A. E. Pazarceviren, A. Tezcaner and Z. Evis, *Microchem. J.*, 2020, **155**, 104713.
86 H. Lee, J. Rho and P. B. Messersmith, *Adv. Mater.*, 2009, **21**, 431–434.
87 H. Lee, S. M. Dellatore, W. M. Miller and P. B. Messersmith, *Science*, 2007, **318**, 426–430.
88 Y. Liu, K. Ai and L. Lu, *Chem. Rev.*, 2014, **114**, 5057–5115.
89 H. Tolabi, N. Bakhtiary, S. Sayadi, M. Tamaddon, F. Ghorbani, A. R. Boccaccini and C. Liu, *Front. Bioeng. Biotechnol.*, 2022, **10**, 1008360.
90 A. S. Arabiyat, M. R. Pfau, M. A. Grunlan and M. S. Hahn, *J. Biomed. Mater. Res., Part A*, 2021, **109**, 2334–2345.
91 R. Teimouri, K. Abnous, S. M. Taghdisi, M. Ramezani and M. Alibolandi, *J. Mater. Res. Technol.*, 2023, **24**, 7938–7973.
92 T. Jacobs, R. Morent, N. D. Geyter, P. Dubruel and C. Leys, *Plasma Chem. Plasma Process.*, 2012, **32**, 1039–1073.
93 A. Morelli and M. J. Hawker, *ACS Biomater. Sci. Eng.*, 2023, **9**, 3760–3777.
94 H. Turkoglu Sasmazel, M. Alazzawi and N. Kadim Abid Alsahib, *Molecules*, 2021, **26**, 1665.
95 Y. Kim and G. Kim, *Colloids Surf., B*, 2014, **125**, 181–189.
96 S. Murab, S. M. S. Gruber, C.-Y. J. Lin and P. Whitlock, *Mater. Sci. Eng., C*, 2020, **109**, 110529.
97 S. Yamada, M. A. Yassin, T. Weigel, T. Schmitz, J. Hansmann and K. Mustafa, *J. Biomed. Mater. Res., Part A*, 2021, **109**, 1560–1574.
98 A. Terriza, J. I. Vilches-Pérez, E. de la Orden, F. Yubero, J. L. Gonzalez-Caballero, A. R. González-Elipe, J. Vilches and M. Salido, *BioMed Res. Int.*, 2014, **2014**, 253590.
99 Q. Song, M. Zhu, Y. Shi, J. Smay and Y. Mao, *ACS Appl. Bio Mater.*, 2023, **6**, 891–898.
100 M. V. Jose, V. Thomas, D. R. Dean and E. Nyairo, *Polymer*, 2009, **50**, 3778–3785.
101 Z. Wang, H. Wang, J. Xiong, J. Li, X. Miao, X. Lan, X. liu, W. Wang, N. Cai and Y. Tang, *Mater. Sci. Eng., C*, 2021, **128**, 112287.
102 N. Amiryaghoubi, N. N. Pesyan, M. Fathi and Y. Omidi, *Colloids Surf., A*, 2022, **634**, 127895.
103 J. Ren, N. Kohli, V. Sharma, T. Shakouri, Z. Keskin-Erdogan, S. Saifzadeh, G. I. Brierly, J. C. Knowles, M. A. Woodruff and E. García-Gareta, *Polymers*, 2021, **13**, 3999.
104 H. Y. Jang, J. Y. Shin, S. H. Oh, J.-H. Byun and J. H. Lee, *ACS Biomater. Sci. Eng.*, 2020, **6**, 5172–5180.
105 M. T. Frassica, S. K. Jones, P. Diaz-Rodriguez, M. S. Hahn and M. A. Grunlan, *Acta Biomater.*, 2019, **99**, 100–109.
106 M. T. Frassica, S. K. Jones, J. Suriboot, A. S. Arabiyat, E. M. Ramirez, R. A. Culibrk, M. S. Hahn and M. A. Grunlan, *Biomacromolecules*, 2020, **21**, 5189–5199.
107 F. O. Beltran, C. J. Houk and M. A. Grunlan, *ACS Biomater. Sci. Eng.*, 2021, **7**, 1631–1639.
108 F. O. Beltran, A. S. Arabiyat, R. A. Culibrk, D. J. Yeisley, C. J. Houk, A. J. Hicks, J. Negrón Hernández, B. M. Nitschke, M. S. Hahn and M. A. Grunlan, *Polymer*, 2023, **284**, 126291.
109 R. Morent, N. D. Geyter, T. Desmet, P. Dubruel and C. Leys, *Plasma Processes Polym.*, 2011, **8**, 171–190.
110 A. Khlyustova, Y. Cheng and R. Yang, *J. Mater. Chem. B*, 2020, **8**, 6588–6609.
111 D. T.-J. Barone, J.-M. Raquez and P. Dubois, *Polym. Adv. Technol.*, 2011, **22**, 463–475.
112 G. A. Rico-Llanos, S. Borrego-González, M. Moncayo-Donoso, J. Becerra and R. Visser, *Polymers*, 2021, **17**, 599.
113 E. Roldán, N. D. Reeves, G. Cooper and K. Andrews, *Front. Bioeng. Biotechnol.*, 2023, **26**, 100452.
114 J. Sun and H. Tan, *Materials*, 2013, **6**, 1285–1309.
115 P. Zhai, X. Peng, B. Li, Y. Liu, H. Sun and X. Li, *Int. J. Biol. Macrmol.*, 2020, **151**, 1224–1239.
116 A. Guzmán-Soria, V. Moreno-Serna, D. A. Canales, C. García-Herrera, P. A. Zapata and P. A. Orihuela, *Polymers*, 2023, **15**, 1079.
117 X. Xue, Y. Han, Y. Deng and J. Su, *Adv. Funct. Mater.*, 2021, **31**, 2009432.
118 L. Yang, S. Pijuan-Galito, H. S. Rho, A. S. Vasilevich, A. D. Eren, L. Ge, P. Habibovic, M. R. Alexander, J. de Boer and A. Carlier, *Chem. Rev.*, 2021, **121**, 4561–4677.
119 A. K. Patel, M. W. Tibbitt, A. D. Celiz, M. C. Davies, R. Langer, C. Denning, M. R. Alexander and D. G. Anderson, *Curr. Opin. Solid State Mater. Sci.*, 2016, **20**, 202–211.
120 M. M. H. Shandhi and J. P. Dunn, *Cell Rep. Med.*, 2022, **3**, 100861.

121 J. L. Guo, M. Januszyk and M. T. Longaker, *Tissue Eng., Part A*, 2023, **29**, 2–19.
122 S. M. McDonald, E. K. Augustine, Q. Lanners, C. Rudin, L. C. Brinson and M. L. Becker, *Nat. Commun.*, 2023, **14**, 4838.
123 A. Logeshwaran, R. Elsen and S. Nayak, *ACS Biomater. Sci. Eng.*, 2024, **10**, 677–696.
124 ISO 23317:2014 – Implants for Surgery – *In Vitro* Evaluation for Apatite-Forming Ability of Implant Materials, 2014.
125 F. Baino and S. Yamaguchi, *Biomimetics*, 2020, **5**, 57.
126 T. Kokubo, *Biomaterials*, 1991, **12**, 155–163.
127 P. X. Zhu, Y. Masuda and K. Koumoto, *J. Colloid Interface Sci.*, 2001, **243**, 31–36.
128 F. Barrere, C. A. van Blitterswijk, K. de Groot and P. Layrolle, *Biomaterials*, 2002, **23**, 1921–1930.
129 J. T. Y. Lee, Y. Leng, K. L. Chow, F. ren, X. Ge, K. Wang and X. Lu, *Acta Biomater.*, 2011, **7**, 2615–2622.
130 M. P. Gashti, F. Alimohammadi, J. Hulliger, M. Burgener, H. Oulevey-Aboulfad and G. L. Bowlin, *Curr. Microsc. Contrib. Adv. Sci. Tech.*, 2012, 625–638.
131 J. Goldstein, D. Newbury, D. Joy, C. Lyman, P. Echlin, E. Lifshin, L. Sawyer and M. Michael, *Scanning Electron Microscopy and X-Ray Microanalysis*, Springer, 3rd edn, 2007, ch. 1, pp. 1–20.
132 J. Jeong, J. H. Kim, J. H. Shim, N. S. Hwang and C. Y. Heo, *Biomater. Res.*, 2019, **23**, 4.
133 R. Kotian, P. P. Rao and P. Madhyastha, *Eur. J. Dent.*, 2017, **11**, 438–446.
134 J. G. M. Poralan, J. E. Gambe, E. M. Alcantara and R. M. Vequizo, *IOP Conf. Series: Mater. Sci. Eng.*, 2015, **79**, 012828.
135 K. Teshima, S. H. Lee, K. Yubuta, S. Mori, T. Shishido and S. Oishi, *CrystEngComm*, 2011, **13**, 827–830.
136 S. Kim, H.-S. Ryu, H. Shin, H. S. Jung and K. S. Hong, *Mater. Chem. Phys.*, 2005, **91**, 500–506.
137 H. Stanjek and W. Häusler, *Hyperfine Interact.*, 2004, **154**, 107–119.
138 M. Mir, F. L. Leiteb, J. P. S. de Paula Herrmann, F. L. Pissettia, A. M. Rossid, E. L. Moreirad and Y. P. Mascarenhase, *Mater. Res.*, 2012, **15**, 622–627.
139 M. Rabiei, A. Palevicius, A. Monshi, S. Nasiri, A. Vilkauskas and G. Janusas, *Nanomaterials*, 2010, **10**, 1627.
140 M. S. Hossain and S. Ahmed, *RSC Adv.*, 2023, **13**, 14625–14630.
141 Y. Cao, M. L. Mei, Q.-L. Li, E. C. M. Lo and C. H. Chu, *ACS Appl. Mater. Interfaces*, 2014, **6**, 410–420.
142 H. Kaur, B. Rana, D. Tomar, S. Kaur and K. C. Jena, in *Modern Techniques of Spectroscopy*, ed. D. K. Singh, M. Pradhan and A. Materny, Springer, Singapore, 2021, pp. 3–56.
143 H. Gheisari, E. Karamian and M. Abdellahi, *Ceram. Int.*, 2015, **41**, 5957–5975.
144 S. G. Kazarian, K. L. A. Chan, V. Maquet and A. R. Boccaccini, *Biomaterials*, 2004, **25**, 3931–3938.
145 L. Borkowski, A. Sroka-Bartnicka, P. Drączkowski, A. Ptak, E. Zięba, A. Ślósarczyk and G. Ginalska, *Mater. Sci. Eng., C*, 2016, **62**, 260–267.
146 K. J. I. Ember, M. A. Hoeve, S. L. McAughtrie, M. S. Bergholt, B. J. Dwyer, M. M. Stevens, K. Faulds, S. J. Forbes and C. J. Campbell, *npj Regener. Med.*, 2017, **2**, 12.
147 M. D. Weir and H. H. K. Xu, *J. Biomed. Mater. Res., Part B*, 2010, **93**, 93–105.
148 S. A. Davari, S. Masjedi, Z. Ferdous and D. Mukherjee, *J. Biophotonics*, 2018, **11**, e201600288.
149 D. N. Misra, *Colloids Surf.*, 1992, **66**, 181–187.
150 C. A. Gregory, W. G. Gunn, A. Peister and D. J. Prockop, *Anal. Biochem.*, 2004, **329**, 77–84.
151 M. Lievremont, J. Potus and B. Guillou, *Acta Anat.*, 1982, **114**, 268–280.
152 M. R. Schneider, *Histochem. Cell Biol.*, 2021, **156**, 523–526.
153 L. F. Bonewald, S. E. Harris, J. Rosser, M. R. Dallas, S. L. Dallas, N. P. Camacho, B. Boyan and A. Boskey, *Calcif. Tissue Int.*, 2003, **72**, 537–547.
154 M. D. Weir and H. H. Xu, *J. Biomed. Mater. Res., Part B*, 2010, **93**, 93–105.
155 K. White, R. Chalaby, G. Lowe, J. Berlin, C. Glackin and R. Olabisi, *Polymers*, 2021, **13**, 2274.
156 B. A. Rahn and S. M. Perren, *Stain Technol.*, 1971, **46**, 125–129.
157 E. Tambutté, S. Tambutté, N. Segonds, D. Zoccola, A. Venn, J. Erez and D. Allemand, *Proc. R. Soc. B*, 2012, **279**, 19–27.
158 A. K. Nguyen, S. B. Nelson, S. A. Skoog, P. Jaipan, P. E. Petrochenko, A. Kaiser, L. Lo, J. Moreno, R. J. Narayan, P. L. Goering and G. Kumar, *J. Biomed. Mater. Res., Part B*, 2023, **111**, 987–995.
159 Y. Kim, E. J. Lee, A. V. Davydov, S. Frukhtbeyen, J. E. Jonathan, S. Takagi, L. Chow and S. Alimperti, *Biomed. Mater.*, 2021, **16**, 045002.
160 D. Lantigua, X. Wu, S. Suvarnapathaki, M. A. Lguyen and G. Camci-Unal, *Bioengineering*, 2021, **8**, 169.
161 Y. Dong, L. Suryani, X. Zhou, P. Muthukumaran, M. Rakshit, F. Yang, F. Wen, A. M. Hassanbhai, K. Parida, D. T. Simon, D. Iandolo, P. S. Lee, K. W. Ng and S. H. Teoh, *Int. J. Mol. Sci.*, 2021, **22**, 6438.
162 K. Vuornos, H. Huhtala, M. Kääriäinen, K. Kuismanen, L. Hupa, M. Kellomäki and S. Miettinen, *J. Biomed. Mater. Res., Part B*, 2019, **108**, 1332–1342.
163 B. Safari, A. Aghanejad, L. Roshangar and S. Davaran, *Colloids Surf., B*, 2021, **198**, 111462.
164 Y.-Z. Jin and J. H. Lee, *Clin. Orthop. Surg.*, 2018, **10**, 271–278.
165 A. J. Friedenstein, R. K. Chailakhyan and U. V. Gerasimov, *Cell Tissue Kinet.*, 1987, **20**, 263–272.
166 A. Arthur and S. Gronthos, *Int. J. Mol. Sci.*, 2020, **21**, 9759.
167 M. J. Poellmann, J. B. Estrada, T. Boudou, Z. T. Berent, C. Franck and A. J. Wagoner Johnson, *J. Biomech. Eng.*, 2015, **137**, 124503.
168 M. Ghasemi, T. Turnbull, S. Sebastian and I. Kempson, *Int. J. Appl. Glass Sci.*, 2021, **22**, 12827.
169 P. Kumar, A. Nagarajan and P. D. Uchil, *Cold Spring Harbor Perspect.*, 2018, 465–468.
170 M. Yuasa, T. Yamada, T. Taniyama, T. Masaoka, W. Xuetao, T. Yoshii, M. Horie, H. Yasuda, T. Uemura, A. Okawa and S. Sotome, *PLoS One*, 2015, **6**, e0116462.

171 J. Mollentze, C. Durandt and M. S. Pepper, *Stem Cells Int.*, 2021, **2021**, 9919361.
172 R. Rosales-Ibáñez, A. E. Viera-Ruiz, J. V. Cauich-Rodríguez, H. J. Carrillo-Escalante, A. González-González, J. J. Rodríguez-Martínez and F. Hernández-Sánchez, *Polym. Bull.*, 2023, **80**, 2533–2552.
173 J. Le, L. Zhongqun, W. Zhaoyan, S. Yijun, W. Yingjin, W. Yaojie, J. Yanan, J. Zhanrong, M. Chunyang and G. Fangli, *Bioact. Mater.*, 2021, **6**, 613–626.
174 W. C. W. Chan, Z. Tan, M. K. T. To and D. Chan, *Int. J. Mol. Sci.*, 2021, **22**, 5545.
175 É. R. Oliveira, L. Nie, D. Podstawczyk, A. Allahbakhsh, J. Ratnayake, D. L. Brasil and A. Shavandi, *Int. J. Mol. Sci.*, 2021, **22**, 903.
176 K. Hu and B. R. Olsen, *Bone*, 2016, **91**, 31–38.
177 S.-Y. Park, K.-H. Kim, S. Kim, Y.-M. Lee and Y.-J. Seol, *Pharmaceutics*, 2019, **11**, 393.
178 H. Cheng, X. Gao, M. Huard, A. Lu, J. J. Ruzbarsky, S. Amra, B. Wang and J. Huard, *Stem Cell Res. Ther.*, 2022, **13**, 385.
179 S. Trivedi, K. Srivastava, A. Gupta, T. S. Saluja, S. Kumar, D. Mehrotra and S. K. Singh, *J. Oral Biol. Craniofac. Res.*, 2020, **10**, 158–160.
180 N. Rezania, M. Asadi-Eydivand, N. Abolfathi, S. Bonakdar, M. Mehrjoo and M. Solati-Hashjin, *J. Mater. Sci.: Mater. Med.*, 2022, **33**, 31.
181 I. L. Tsiklin, A. V. Shabunin, A. V. Kolsanov and L. T. Volova, *Polymers*, 2022, **14**, 3222.
182 Y. Li, S.-K. Chen, L. Li, L. Qin, X.-L. Wang and Y.-X. Lai, *J. Orthop. Translat.*, 2015, **3**, 95–104.
183 D. S. Sparks, S. Saifzadeh, F. M. Savi, C. E. Dlaska, A. Berner, J. Henkel, J. C. Reichert, M. Wullschleger, J. Ren, A. Cpitria, J. A. McGovern, R. Steck, M. Wagels, M. A. Woodruff, M. A. Schuetz and D. W. Hutmacher, *Nat. Protoc.*, 2020, **15**, 877–924.
184 P. P. Spicer, J. D. Kretlow, S. Young, J. A. Jansen, F. K. Kasper and A. G. Mikos, *Nat. Protoc.*, 2012, **7**, 1918–1929.
185 J. Zurlo, D. Rudacille and A. M. Goldberg, *Altern. Lab Anim.*, 1996, **23**, 298–304.
186 T. El Khassawna, F. Merboth, D. Malhan, W. Böcker, D. E. Daghma, S. Stoetzel, S. Kern, F. Hassan, D. Rosenbaum and J. Langenstein, *Am. J. Pathol.*, 2017, **187**, 1686–1699.
187 M. Rupp, C. Biehl, D. Malhan, F. Hassan, S. Attia, S. Rosch, A. B. Schäfer, E. McMahon, M. Kampschulte, C. Heiss and T. El Khassawna, *Life*, 2021, **11**, 254.
188 E. Ortona, M. T. Pagano, L. Capossela and W. Malorni, *Biology*, 2023, **12**, 993.
189 S. Freitas-Ribeiro, R. L. Reis and R. P. Pirraco, *PNAS Nexus*, 2022, **1**, 1–15.
190 E. A. Fragogeorgi, M. Rouchota, M. Georgiou, M. Velez, P. Bouziotis and G. Loudos, *J. Tissue Eng.*, 2019, **10**, 2041731419854586.
191 M. Ventura, O. C. Boerman, C. de Korte, M. Rijpkema, A. Heerschap, E. Oosterwijk, J. A. Jansen and X. F. Walboomers, *Tissue Eng.*, 2014, **20**, 578–595.
192 J. D. Boerckel, D. E. Mason, A. M. McDermott and E. Alsberg, *Stem Cell Res. Ther.*, 2014, **5**, 144.
193 M. P. Fernández, F. Witte and G. Tozzi, *J. Microscopy*, 2020, **277**, 179–196.
194 E. L. Ritman, *Annu. Rev. Biomed. Eng.*, 2011, **13**, 531–552.
195 E. F. Morgan, A. d Giacomo and L. C. Gerstenfeld, in *Skeletal Development and Repair: Methods and Protocols, Methods in Molecular Biology*, ed. M. J. Hilton, Springer Nature, 2021, pp. 17–37.
196 S. Bastawrous, P. Bhargava, F. Behnia, D. S. W. Djang and D. R. Haseley, *Nucl. Med.*, 2014, **34**, 1295–1316.
197 K. Horiuchi-Suzuki, A. Konno, M. Udeda, Y. Fukuda, S. Nishio, K. Hashimoto and H. Saji, *Eur. J. Nucl. Med. Mol. Imaging*, 2004, **31**, 388–398.
198 S. Annibali, D. Bellavia, L. Ottolenghi, A. Cicconettie, M. P. Cristalli, R. Quaranta and A. Pilloni, *J. Biomed. Mater. Res., Part B*, 2014, **102**, 815–825.
199 M. Ventura, G. M. Franssen, E. Oosterwijk, O. C. Boerman, J. A. Jansen and X. F. Walboomers, *J. Tissue Eng. Regener. Med.*, 2016, **10**, 843–854.
200 H. S. Kim, E. S. Jeong, M. H. Yang and S.-O. Yang, *Osteoporosis Sarcopenia*, 2018, **4**, 79–85.
201 B. Gurumurthy, M. A. Tucci, L.-W. Fan, H. A. Benghuzzi, P. Pal, G. L. Bidwell, S. M. S. Moracho, Z. Cason, D. Gordy and A. V. Jonorkar, *Adv. Healthcare Mater.*, 2020, **9**, 1901385.
202 C.-C. Niu, S.-S. Lin, W.-J. Chen, S.-J. Liu, L.-H. Chen, C.-Y. Yang, C.-J. Wang, L.-J. Yuan, P.-H. Chen and H.-Y. Cheng, *J. Orthop. Surg. Res.*, 2015, **10**, 111.
203 G. Chang, S. Boones, D. Martel, C. S. Rajapaske, R. S. Hallyburton, M. Valko, S. Honig and R. R. Regatte, *J. Magn. Reson. Imaging*, 2017, **46**, 323–337.
204 E. J. Ribot, C. Tournier, R. Aid-Launais, N. Koonjoo, H. Oliveira, A. J. Trotier, S. Rey, D. Wecker, D. Letourneur, J. A. Vilamitjana and S. Miraux, *Sci. Rep.*, 2017, **7**, 6100.
205 S. Tang, P. Shajudeen, E. Tasciotti and R. Righetti, *Sci. Rep.*, 2020, **10**, 13646.
206 F. A. Shah, K. Ruscsák and A. Palmquist, *Bone Res.*, 2019, **7**, 15.
207 N. Celikkin, S. Mastrogiacomo, W. Dou, A. Heerschap, E. Oosterwijk, X. F. Walboomers and W. Święszkowski, *J. Biomed. Mater. Res.*, 2022, **110**, 2133–2145.
208 J. J. Jolly, N. F. M. Fozi, K.-Y. Chin, S. K. Wong, K. H. Chua, E. Alias, N. S. Adnan and S. Ima-Nirwana, *Exp. Ther. Med.*, 2021, **22**, 680.
209 K. Oe, M. Miwa, K. Nagamune, Y. Sakai, S. Y. Lee, T. Niikura, T. Iwakura, T. Hasegawa, N. Shibanuma, Y. Hata, R. Kuroda and M. Kurosaka, *Tissue Eng.*, 2010, **16**, 347–353.
210 L. Borkowski, A. Sroka-Bartnicka, I. Polkowska, M. Pawlowska, K. Palka, E. Zieba, A. Slosarczyk, K. Jozwiak and G. Ginalska, *Anal. Bioanal. Chem.*, 2017, **409**, 5747–5755.
211 M. Fraulob, S. Pang, S. L. Cann, R. Vayron, M. Laurent-Brocq, S. Todatry, J. A. N. T. Soares, I. Jasiuk and G. Haïat, *Med. Eng. Phys.*, 2020, **84**, 60–67.
212 F. Rauch, in *Osteogenesis Imperfecta: A Translational Approach to Brittle Bone Disease*, ed. J. R. Shapiro,

P. H. Byers, F. H. Glorieux and P. D. Sponseller, Academic Press, 2014, pp. 237–242.
213 D. Malhan, M. Muelke, S. Rosch, A. B. Schaefer, F. Merboth, D. Weisweiler, C. Heiss, I. Arganda-Carreras and T. E. Khassawana, *Front. Endocrinol.*, 2018, **9**, 666.
214 F. M. Savi, F. Lawrence, D. W. Hutmacher, M. A. Woodruff, L. J. Bray and M. L. Wille, *Tissue Eng., Part C*, 2019, **25**, 732–741.
215 K. P. Egan, T. A. Brennan and R. J. Pignolo, *Histopathology*, 2012, **61**, 1168–1173.
216 A. H. Fischer, K. A. Jacobson, J. Rose and R. Zeller, *Cold Spring Harbor Perspect.*, 2008, **2008**, pdb.prot4986.
217 W. Bloch and Y. Korkmaz, *Classical histological staining procedures in cardiovascular research*, 2005.
218 F. Shapiro and J. Y. Wu, *Eur. Cell. Mater.*, 2019, **38**, 137–167.
219 S. Wulff, L. Hafer, M. Cheles, D. A. Htl and D. A. Stanforth, Guide to special stains, 2004.
220 C. Zhang, B. Yan, Z. Cui, S. Cui, T. Zhang, X. Wang, D. Liu, R. Yang, N. Jiang and Y. Zhou, *Sci. Rep.*, 2017, **7**, 10519.
221 N. N. F. N. M. N. Kahar, M. Jaafar, N. Ahmad, A. R. Sulaiman, B. H. Yahaya and Z. A. A. Hamid, *Mater. Today: Proc.*, 2022, **66**, 3031–3035.
222 Y. Niu, T. Du and Y. Liu, *J. Funct. Biomater.*, 2023, **14**, 212.
223 C. G. Helguero, V. M. Mustahsan, S. Parmar, S. Pentyala, J. L. Pfail, I. Kao, D. E. Komatsu and S. Pentyala, *J. Orthop. Surg. Res.*, 2017, **12**, 195.
224 ISO 604:2002 – Plastics – Determination of Compressive Properties, 2002.
225 C. G. Helguero, J. L. Amaya, D. E. Komatsu, S. Pentyala, V. Mustahsan, E. A. Ramirez and I. Kao, *Proceedia CIRP*, 2017, **65**, 121–126.
226 ISO 5833:2022 – Implants for surgery – Acrylic resin cements, 2022.
227 D. Wu, A. Spanou, A. Diez-Escudero and C. Persson, *J. Mech. Behav. Biomed. Mater.*, 2020, **103**, 103608.
228 Z. T. Lawson, J. Han, W. B. Saunders, M. A. Grunlan, M. R. Moreno and A. R. Robbins, *Methods X*, 2021, **8**, 101541.
229 P. J. Thurner, *Wiley Interdiscip. Rev.: Nanomed. Nanobiotechnol.*, 2009, **1**, 624–649.
230 M. Bontempi, F. Salamnna, R. Capozza, A. Visani, M. Fini and A. Gambardella, *Materials*, 2022, **15**, 7512.
231 Y. Zhou and J. Du, *Prog. Biophys. Mol. Biol.*, 2022, **176**, 52–66.
232 C. Su, J. Shi, Y. Hu, S. Hu and J. Ma, *US Pat.*, US9291640B2, 2014.
233 Y. Zhou, M. Kastner, T. B. Tighe and J. Du, *Extreme Mech. Lett.*, 2020, **41**, 101031.
234 Y. Zhou, C. Gong, M. Hossaini-Zadeh and J. Du, *J. Mech. Behav. Biomed. Mater.*, 2020, **110**, 103858.
235 C. G. Simon, M. J. Yaszmeski, A. Ratcliffe, P. Tomlins, R. Luginbuehl and J. A. Tesk, *J. Biomed. Mater. Res., Part B*, 2015, **103**, 949–959.
236 E. E. A. Cramer, K. Ito and S. Hofmann, *Curr. Osteoporos. Rep.*, 2021, **19**, 75–87.

